JOURNAL
OF THE
WASHINGTON ACADEMY OF SCIENCES
VOL. 44 June 1954 No. 6

# PHYSICS.—*Some newly solved and some unsolved problems in optics.*[1]

A. I. MAHAN, U. S. Naval Ordnance Laboratory, White Oak, Md.

This evening I should like to discuss some new optical problems that arose during the war years. Some of these were solved, but others still remain unsolved. Previously, I have discussed certain parts of these problems with various technical groups. I am particularly glad to have the opportunity to present to you a more complete story. In this lecture I will discuss particularly the experimental problems and the significance of the results and will minimize the mathematics involved.

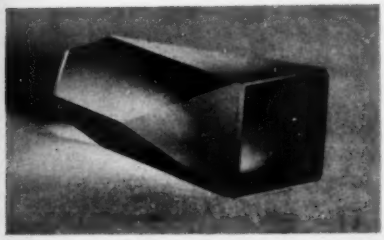

FIG. 1.—Photograph of three internal reflection roof prism.

The story starts with the rather unusual prism shown in Fig. 1. This is one of a general class of prisms commonly referred to as roof prisms, because of the roof- or gablelike structure on the side of the prism seen at the left. To function properly this roof angle, on the more usual type roof prisms, must be 90° within 2 or 3 seconds. The geometry of this prism and the manner in which it is used can be seen more clearly in Fig. 2. Light from the lower right in the figure enters the first prism face normally and then falls on the roof at the top of the figure. The indicated light ray may either strike the lower roof surface and then the upper or the upper and then the lower, depending upon whether it is incident in the lower or upper half of the prism aperture. After leaving the roof surface, the indicated ray again undergoes another reflection at an angle of 60° and then emerges from the prism in a horizontal direction at the left. The function of this prism is that of inverting the image of a distant object in a direction normal to the plane of the figure and deviating the light through an angle of 120°. This prism formed an important part of one of our ordnance instruments.

When we attempted to make this particular prism a new optical problem appeared. The sequence of events leading up to the discovery of this problem was as follows: Suppose first that we place a cross, illuminated by monochromatic light, in a plane normal to the incident ray in Fig. 2 at a large distance from the prism, so that one arm of this cross lies in the plane of the figure and the other lies perpendicular to the plane of the figure. If now we look from the left through this prism at the illuminated cross with a high-power telescope (about 16 power) the arm of the cross in the plane of this figure appeared doubled, while the other arm of the cross, perpendicular to this

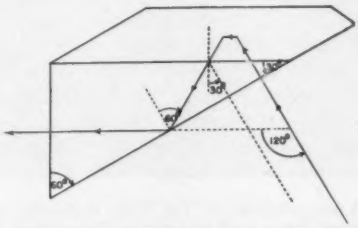


FIG. 2.—Ray diagram for three internal reflection roof prism.

[1] Retiring Presidential Address, Philosophical Society of Washington, delivered on January 15, 1954.

Dedicated to my parents Mr. and Mrs. A. E. Mahan.

plane, appeared single and sharp. Anyone who has worked with other types of roof prisms knows that such a doubling of the image can quite readily be produced by making errors in the roof angle, so that it deviates from the usual 90°. Attempts were made to increase the accuracy in this roof angle. Prisms were made in pairs in the following manner: Two roof surfaces from separate prisms were first ground and polished to a tenth of a wavelength or better and then optically placed in contact. Two such prisms, when contacted in this way, are very firmly bound together and can be treated as a single piece of glass. The second roof surfaces of each of these two prisms were then ground and polished as a single surface, and periodic tests were made on the roof angle on one of these prisms to determine when it was as near 90° as could be measured. Such a technique of making these roof angles assured us that these angles were at least supplementary. When, however, the two prisms were separated and the cross viewed through the prisms as before, the same doubling appeared in both of these prisms. The late Max Zwillinger of our staff suggested that we coat the roof surfaces with silver. We were very much surprised at the result, for the doubling of the image disappeared in both prisms, and two apparently rather poor prisms were transformed into two very good roof prisms.

I must be careful to state at this point that the same type of observation was also made in Germany at about the same time we were making our observations here. Prof. G. Joos at the Zeiss Works in Germany had found that the more usual 90° deviation Amici Roof Prism, which will be discussed later, also exhibited the same behavior but to a much smaller degree and that again silvering helped in minimizing this image doubling. Professor Joos in his report, however, concerned himself more with the polarization properties of such prisms and made no attempt to calculate the forms of the image.[2]

[2] I am indebted to Dr. I. C. Gardner, of the National Bureau of Standards, for calling attention to this publication in the Zeiss Nachrichten 4: 9, 1943.

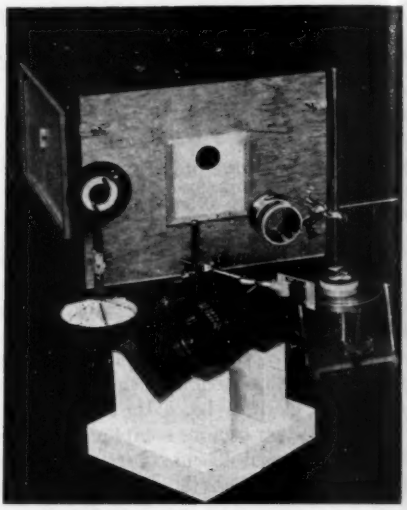

FIG. 3.—Photograph of apparatus used for testing three internal reflection roof prism.

Our first studies of the phenomenon were confined more to actual experimental observations. We tried, for example, to photograph the phenomenon both in and out of the focal plane of a long focal length lens. For this purpose we assembled apparatus of the form shown in Fig. 3. A cross made of lines 0.01 mm wide, ruled on a silvered glass plate, was mounted behind the hole in the box at the left and illuminated by 5461 A° light from an AH4 high-pressure mercury arc. This light was then collimated by a 500-mm E.F. telescopic objective and permitted to be incident on the prism in the manner suggested in Fig. 2. After emerging from the prism, the light was brought to a focus by a 2839 mm E.F. lens. Pictures were then taken both in the focal plane of the lens and at various distances to both sides. The results of these photographs are shown in Fig. 4. In the column at the left can be seen the images of the cross obtained when recorded through the unsilvered prism, and on the right are the corresponding images of the cross photographed through the prism with silvered roof surfaces. The position indicated by D = 0 corresponds to the focal plane. If you look carefully at the horizontal lines in both of these images, you will see that the hori-

A. I. MAHAN, President of the Philosophical Society of Washington, 1953

zontal line in the image recorded through the unsilvered prism appears doubled, while the corresponding horizontal line through the silvered prism appears single and sharp. Both of the vertical lines appear of the same sharpness and of about the same breadth as the horizontal line for the silvered prism. The particular problem in which we were interested, then, was why this doubling of the image in the horizontal direction, seen through the unsilvered prism, should disappear when the roof surfaces were coated with silver. As the film was moved away from the focal plane in both directions figures of the forms indicated above and below the position marked $D = 0$ were found. The horizontal line of the image for the unsilvered prism separates more distinctly into two separate images with increasing distances from the focal plane. The corresponding horizontal line for the silvered prism shows the same tendency to separate into two separate images, but this separation is not so distinct as that for the unsilvered prism. The vertical lines in both types of prisms show the same type of image behavior.

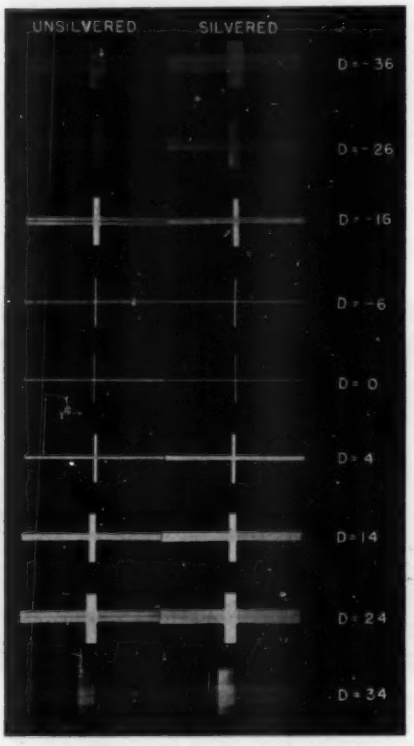


FIG. 4.—Photograph of images for three internal reflection roof prism when roof surfaces are both coated with silver and uncoated.

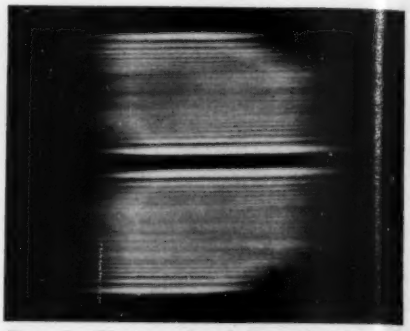

FIG. 5.—Photograph of Fresnel Diffraction Pattern for uncoated three internal reflection roof prism.

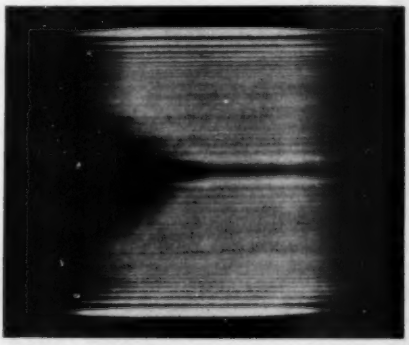

FIG. 6.—Photograph of Fresnel Diffraction Pattern for silver coated three internal reflection roof prism.

If you will look carefully at both sets of images you may be able to see narrow sets of parallel lines resembling diffraction patterns. To show more what these look like at large distances from the focal plane, we have included two additional figures. In the first of these (see Fig. 5) we have shown a section of the horizontal line for the unsilvered prism. You will see now that the upper and lower halves of the aperture produce their own Fresnel Diffraction Patterns. In Fig. 6 is the corresponding photograph of the Fresnel Diffraction Pattern for the prism with silvered roof surfaces.

Both halves of the prism again produce their own Fresnel Diffraction Patterns, but in the center they seem now to interact so that simultaneously the prism also tends to produce a diffraction pattern characteristic of the whole aperture, rather than just half.

The previous photographs suggested very strongly that this phenomenon was some sort of a diffraction problem. We therefore returned to the focal plane and tried to enlarge the diffraction pattern in this vicinity. To do this we made use of a 5-mm square aperture, which can be seen already in place in Fig. 3 behind the prism. This aperture was placed normal to the emerging ray in Fig. 2 in such a manner that the plane containing the roof edge bisected one pair of parallel sides of the aperture. The resulting diffraction pattern when enlarged is that shown in Fig. 7. This picture, although somewhat over exposed, still shows the characteristics of the diffraction pattern. In addition to the doubling of the horizontal line at the center of the pattern, the bands in the outer structure are twice as wide and twice as far apart when compared with the spacing of the bands in the vertical direction. The first part of the problem which had to be understood was then why the diffraction pattern for the unsilvered prism takes this particular shape.

FIG. 7.—Photograph of diffraction pattern in focal plane for three internal reflection roof prism with uncoated surfaces.

To explain these unusual imaging properties a rather detailed theoretical and experimental program was undertaken. This work was carried out in two separate phases. The first phase of the problem consisted largely of an experimental and theoretical study of the particular properties of the prism already described. Using classical electromagnetic theory, attempts were made to calculate the forms of the diffraction patterns both in polarized and unpolarized light when the roof surfaces of the prism were uncoated. Without quantitative measurements about all that we could say was that the calculated and experimentally observed patterns seemed to be of the same general forms. Nothing was done about calculating the forms of the diffraction patterns when the roof surfaces were coated with silver. These papers, however, opened up a problem of a considerably more general nature. We were frequently asked the question, "Do all roof prisms exhibit this same type of behavior?" About all that we could say was that there was evidence for thinking that they might, but we could not give any data or theoretical calculations to justify our remarks. During the second phase of the problem, I was very fortunate to have Edward Price[3] as an associate. Mr. Price spent large amounts of time and energy in making many experimental observations and photographs of these phenomena and relating the experimental data to the theoretically calculated data. The success of this phase of the work is due in a large measure to his interest and industry. In this second phase of the problem, the theoretical considerations were reopened with the view of extending them to all types of roof prisms, when their roof surfaces were either uncoated or coated. These theoretical considerations led us to some very general equations for these roof prisms. As an example of these equations, careful quantitative measurements were made on the diffraction pattern for the 90° deviation Amici Roof Prism, when its roof surfaces were both uncoated and coated with silver. In this paper it will be my purpose to describe to you in a general way the nature of these considerations and the results which we obtained.

## POLARIZATION PROPERTIES OF ROOF PRISMS WITH UNCOATED REFLECTING ROOF SURFACES

It might be rather surprising that we found it necessary to bring polarized light

[3] Now resident naval inspector of ordnance at Arma Corporation, Brooklyn, N. Y.

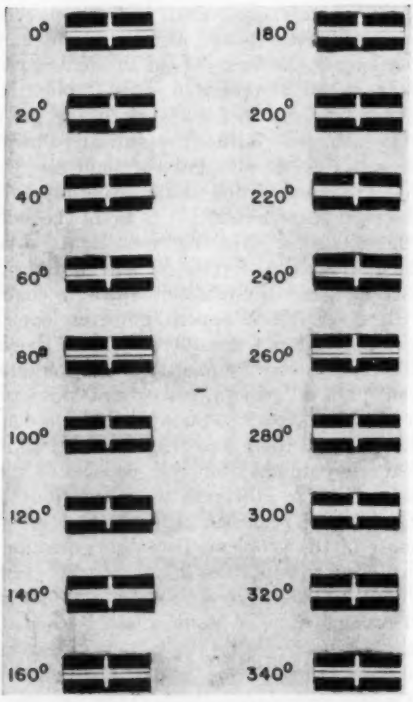


FIG. 8.—Photograph of diffraction pattern in focal plane for three internal reflection roof prism with uncoated surfaces when illuminated by plane polarized light of varying azimuth angles.

into the discussion, for in use, roof prisms are normally illuminated with unpolarized light. Experimentally, however, we found the rather interesting fact that when plane polarized light was allowed to enter the prism shown in Figs. 1 and 2, light of different ellipticities emerged from the upper and lower halves of the aperture. We found also that the form of the diffraction pattern could be altered very markedly by simply changing the entering azimuth angle of the plane polarized light. If in Fig. 3 we place the polarizing element between the prism and the collimating lens and simply rotate this polarizing element, we find the diffraction patterns to undergo the changes shown in Fig. 8. For an azimuth angle 0°, a satellite appears on the upper side of the horizontal central diffraction band. As the azimuth angle is increased, this satellite gradually merges into the parent line, and then reappears below the parent line. Additional increases in the azimuth angle cause this satellite to again merge into the parent line and to reappear on the upper side. This phenomenon is such that for every 180° rotation of the polarizing element, the diffraction pattern repeats itself. No noticeable changes take place in the vertical diffraction pattern. This behavior was totally unexpected but nevertheless had to be understood if we were to explain fully the peculiar behavior of this prism.

In trying to understand the reasons for these peculiar imaging properties we learned that the most important consideration was what happens at the two reflecting roof surfaces. We therefore set out first to determine the geometry of all the rays and the perpendicular and parallel components of the electric vector at each of the reflecting roof surfaces. To make these considerations valid for all types of roof prisms, we visualized a general roof prism of the form shown in Fig. 9 in which the angular deviation at the roof edge $D$ could have any arbitrary value. We also constructed a general roof prism model of the form shown in Fig. 10. In this model, the strings represented the light rays and the matches the perpendicular and parallel components of the electric

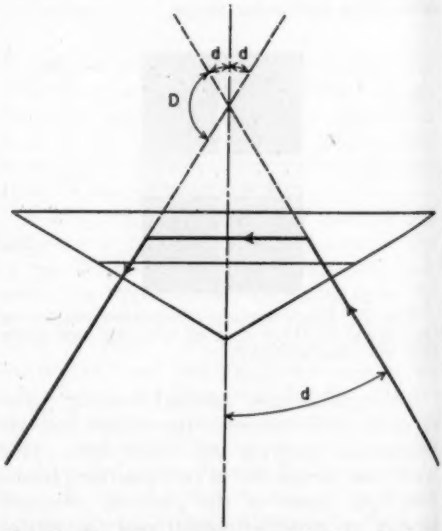


FIG. 9.—Ray diagram for generalized roof prism.

TABLE I. Direction cosines of incident rays, reflected rays, "$s$" and "$p$" vibrations and equations of planes of incidence for rays entering upper half of prism aperture and emerging from lower.

| | | | |
|---|---|---|---|
| Equation of first plane of incidence $(\cos\frac{1}{2}D)x+(\cos\frac{1}{2}D)y+(\sin\frac{1}{2}D)z=0$ | | | |
| Incident ray | $+\sin\frac{1}{2}D$ | $0$ | $-\cos\frac{1}{2}D$ |
| Surface normal | $+\frac{1}{\sqrt{2}}$ | $-\frac{1}{\sqrt{2}}$ | $0$ |
| Reflected ray | $0$ | $-\sin\frac{1}{2}D$ | $+\cos\frac{1}{2}D$ |
| $S_1$ | $+\frac{\cos\frac{1}{2}D}{(\cos^2\frac{1}{2}D+1)^{\frac{1}{2}}}$ | $+\frac{\cos\frac{1}{2}D}{(\cos^2\frac{1}{2}D+1)^{\frac{1}{2}}}$ | $+\frac{\sin\frac{1}{2}D}{(\cos^2\frac{1}{2}D+1)^{\frac{1}{2}}}$ |
| $P_1$ before reflection | $+\frac{\cos^2\frac{1}{2}D}{(\cos^2\frac{1}{2}D+1)^{\frac{1}{2}}}$ | $-\frac{1}{(\cos^2\frac{1}{2}D+1)^{\frac{1}{2}}}$ | $+\frac{\sin\frac{1}{2}D\cos\frac{1}{2}D}{(\cos^2\frac{1}{2}D+1)^{\frac{1}{2}}}$ |
| $P_1$ after reflection | $+\frac{1}{(\cos^2\frac{1}{2}D+1)^{\frac{1}{2}}}$ | $-\frac{\cos^2\frac{1}{2}D}{(\cos^2\frac{1}{2}D+1)^{\frac{1}{2}}}$ | $-\frac{\sin\frac{1}{2}D\cos\frac{1}{2}D}{(\cos^2\frac{1}{2}D+1)^{\frac{1}{2}}}$ |
| Equation of second plane of incidence $(\cos\frac{1}{2}D)x-(\cos\frac{1}{2}D)y-(\sin\frac{1}{2}D)z=0$ | | | |
| Incident ray | $0$ | $+\sin\frac{1}{2}D$ | $-\cos\frac{1}{2}D$ |
| Surface normal | $+\frac{1}{\sqrt{2}}$ | $+\frac{1}{\sqrt{2}}$ | $0$ |
| Reflected ray | $+\sin\frac{1}{2}D$ | $0$ | $+\cos\frac{1}{2}D$ |
| $S_2$ | $-\frac{\cos\frac{1}{2}D}{(\cos^2\frac{1}{2}D+1)^{\frac{1}{2}}}$ | $+\frac{\cos\frac{1}{2}D}{(\cos^2\frac{1}{2}D+1)^{\frac{1}{2}}}$ | $+\frac{\sin\frac{1}{2}D}{(\cos^2\frac{1}{2}D+1)^{\frac{1}{2}}}$ |
| $P_2$ before reflection | $+\frac{1}{(\cos^2\frac{1}{2}D+1)^{\frac{1}{2}}}$ | $+\frac{\cos^2\frac{1}{2}D}{(\cos^2\frac{1}{2}D+1)^{\frac{1}{2}}}$ | $+\frac{\sin\frac{1}{2}D\cos\frac{1}{2}D}{(\cos^2\frac{1}{2}D+1)^{\frac{1}{2}}}$ |
| $P_2$ after reflection | $+\frac{\cos^2\frac{1}{2}D}{(\cos^2\frac{1}{2}D+1)^{\frac{1}{2}}}$ | $+\frac{1}{(\cos^2\frac{1}{2}D+1)^{\frac{1}{2}}}$ | $-\frac{\sin\frac{1}{2}D\cos\frac{1}{2}D}{(\cos^2\frac{1}{2}D+1)^{\frac{1}{2}}}$ |
| Vertical $S_2$ vibration | $0$ | $-1$ | $0$ |
| Horizontal $P_2$ vibration | $-\cos\frac{1}{2}D$ | $0$ | $+\sin\frac{1}{2}D$ |

TABLE II. Direction cosines of incident rays, reflected rays, "$s$" and "$p$" vibrations and equations of planes of incidence for rays entering lower half of prism aperture and emerging from upper.

| | | | |
|---|---|---|---|
| Equation of first plane of incidence $(\cos\frac{1}{2}D)x-(\cos\frac{1}{2}D)y+(\sin\frac{1}{2}D)z=0$ | | | |
| Incident ray | $+\sin\frac{1}{2}D$ | $0$ | $-\cos\frac{1}{2}D$ |
| Surface normal | $+\frac{1}{\sqrt{2}}$ | $+\frac{1}{\sqrt{2}}$ | $0$ |
| Reflected ray | $0$ | $+\sin\frac{1}{2}D$ | $+\cos\frac{1}{2}D$ |
| $S_1'$ | $-\frac{\cos\frac{1}{2}D}{(\cos^2\frac{1}{2}D+1)^{\frac{1}{2}}}$ | $+\frac{\cos\frac{1}{2}D}{(\cos^2\frac{1}{2}D+1)^{\frac{1}{2}}}$ | $-\frac{\sin\frac{1}{2}D}{(\cos^2\frac{1}{2}D+1)^{\frac{1}{2}}}$ |
| $P_1'$ before reflection | $+\frac{\cos^2\frac{1}{2}D}{(\cos^2\frac{1}{2}D+1)^{\frac{1}{2}}}$ | $+\frac{1}{(\cos^2\frac{1}{2}D+1)^{\frac{1}{2}}}$ | $+\frac{\sin\frac{1}{2}D\cos\frac{1}{2}D}{(\cos^2\frac{1}{2}D+1)^{\frac{1}{2}}}$ |
| $P_1'$ after reflection | $+\frac{1}{(\cos^2\frac{1}{2}D+1)^{\frac{1}{2}}}$ | $+\frac{\cos^2\frac{1}{2}D}{(\cos^2\frac{1}{2}D+1)^{\frac{1}{2}}}$ | $-\frac{\sin\frac{1}{2}D\cos\frac{1}{2}D}{(\cos^2\frac{1}{2}D+1)^{\frac{1}{2}}}$ |
| Equation of second plane of incidence $(\cos\frac{1}{2}D)x+(\cos\frac{1}{2}D)y-(\sin\frac{1}{2}D)z=0$ | | | |
| Incident ray | $0$ | $-\sin\frac{1}{2}D$ | $-\cos\frac{1}{2}D$ |
| Surface normal | $+\frac{1}{\sqrt{2}}$ | $-\frac{1}{\sqrt{2}}$ | $0$ |
| Reflected ray | $+\sin\frac{1}{2}D$ | $0$ | $+\cos\frac{1}{2}D$ |
| $S_2'$ | $+\frac{\cos\frac{1}{2}D}{(\cos^2\frac{1}{2}D+1)^{\frac{1}{2}}}$ | $+\frac{\cos\frac{1}{2}D}{(\cos^2\frac{1}{2}D+1)^{\frac{1}{2}}}$ | $-\frac{\sin\frac{1}{2}D}{(\cos^2\frac{1}{2}D+1)^{\frac{1}{2}}}$ |
| $P_2'$ before reflection | $+\frac{1}{(\cos^2\frac{1}{2}D+1)^{\frac{1}{2}}}$ | $-\frac{\cos^2\frac{1}{2}D}{(\cos^2\frac{1}{2}D+1)^{\frac{1}{2}}}$ | $+\frac{\sin\frac{1}{2}D\cos\frac{1}{2}D}{(\cos^2\frac{1}{2}D+1)^{\frac{1}{2}}}$ |
| $P_2'$ after reflection | $+\frac{\cos^2\frac{1}{2}D}{(\cos^2\frac{1}{2}D+1)^{\frac{1}{2}}}$ | $-\frac{1}{(\cos^2\frac{1}{2}D+1)^{\frac{1}{2}}}$ | $-\frac{\sin\frac{1}{2}D\cos\frac{1}{2}D}{(\cos^2\frac{1}{2}D+1)^{\frac{1}{2}}}$ |
| Vertical $S_2'$ vibration | $0$ | $-1$ | $0$ |
| Horizontal $P_2'$ vibration | $-\cos\frac{1}{2}D$ | $0$ | $+\sin\frac{1}{2}D$ |

vector at each of the reflecting surfaces. A single match appearing first on the string at the right represents the electric vector of the incident plane polarized light. A sign, convention, of course, had to be adopted, and so the unlighted ends of the matches were in each case pointed in the assumed positive directions. The matches and strings could also be removed and mounted in such a way that the incident light ray entered the lower half of the prism aperture and emerged from the upper. These studies led to the formation of two tables of direction cosines indicated as Tables I and II. In the first of these, the direction cosines given for all the rays, surface normals, and perpendicular and parallel components of the electric vector are those for the case in which the light is incident in the upper half of the aperture and emerges from the lower. Table II gives the corresponding values for these direction cosines when the incident light enters the lower half of the prism aperture and emerges from the upper. It should be emphasized at this point that these tables apply only to rays in Fig. 9 which are normal to the entering surface of the generalized prism and hence are incident on the two roof surfaces at the same angle of incidence. With such tables it is now possible, by utilizing the usual cosine law, to determine the various azimuth angles and the angle of incidence on each of the roof surfaces. All of these quantities have been expressed in terms of the angle D so that the magnitudes of these various angles will be known for any prism of arbitrary angular deviation $D$ at the roof edge.

These roof surfaces make another interesting contribution to this problem. At each of the roof surfaces for all roof prisms, the angle of incidence is larger than the critical angle. According to classical electromagnetic theory, all the light incident on such a glass-air surface beyond the critical angle is reflected. After reflection, however, there is a change in phase and this change in phase is different for the parallel and perpendicular components of the electric vector. (*1*). To determine the ellipticity of the light emerging from the lower half of such a prism, one must consider what happens in succession at the two reflecting

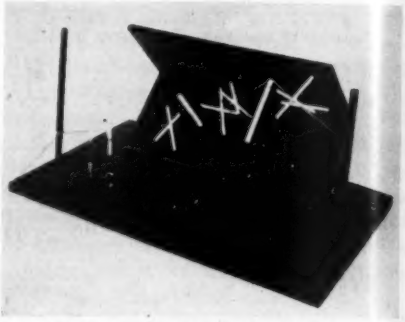

FIG. 10.—Generalized roof prism model.

surfaces. The incident electric vector must first be resolved into parallel and perpendicular components at the upper roof surface in Fig. 10 so that the phase changes at this surface can be added to each of these two components. Both of these components, after reflection at the upper roof surface, are then incident upon the lower roof surface at the same angle of incidence. However, if you look at the model you will see that the parallel and perpendicular components of the electric vector at the lower surface are oriented in different directions from those at the upper surface. To add the phase changes characteristic of the lower surface, the two components of the electric vector from the upper surface must then be resolved about the parallel and perpendicular directions for the lower roof surface. This same procedure also is necessary for light entering the lower half of the prism aperture. For a value of $D = 90°$, the relative orientations of the perpendicular and parallel components, after reflection at the second roof surface along the two paths through the prism can be seen at the left in Fig. 11. Later we are going to be interested in how the emergent light waves in the upper and lower halves of the aperture interact. It therefore becomes necessary to resolve each of these pairs of components in the two halves of the aperture about perpendicular directions[4] which are parallel

[4] These directions are chosen because most of the conventional three internal reflection roof prisms have their third reflecting surface perpendicular to the base of the model and these directions would then correspond to the incident parallel and perpendicular components for such a surface.

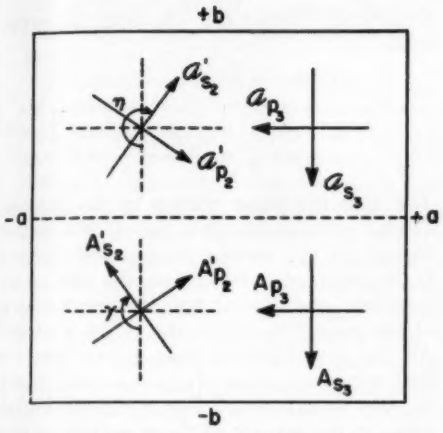


FIG. 11.—Directions of vibration of perpendicular and parallel components of electric vector at the 2-second reflecting roof surfaces for a 90° deviation roof prism, and the final directions about which they were resolved in the emerging aperture.

to each other in the two halves of the aperture as indicated at the right in this figure.

To arrive at expressions for the $A_{s3}$ and the $A_{p3}$ waves emerging from the lower half of the prism aperture, it is necessary to do mathematically what we have just stated in words. If we assume a plane polarized light wave having the electric vector $A_0 \sin(\omega t + d_i)$ to be incident on the prism, it must first be resolved into perpendicular and parallel components at the upper roof surface in Fig. 10. The phase changes which occur after reflection can then be added for each of these waves. These two waves are then incident on the lower roof surface and must be resolved about the perpendicular and parallel directions for this surface so that the phase changes after reflection can be added. Finally the two components after reflection at the lower roof surface must be resolved about the two perpendicular directions indicated at the right in Fig. 11. After these operations have been carried out step by step, the following equations were found for the final two perpendicular components of the electric vector emerging from the lower half of the prism aperture:

$$\begin{aligned} A_{s3} = A_0\{&\cos^2\alpha(\cos^2\beta\cos^2\gamma + \sin^2\beta\sin^2\gamma \\ &+ \sin^2\alpha(\sin^2\beta\cos^2\gamma + \cos^2\beta\sin^2\gamma) \\ &- \tfrac{1}{2}\sin 2\alpha\sin 2\beta\cos 2\gamma\cos(d_{s_1} - d_{p_1}) \\ &- \sin 2\gamma[\cos^2\alpha\cos^2\beta + \sin^2\alpha\sin^2\beta \\ &- \tfrac{1}{2}\sin 2\alpha\sin 2\beta\cos(d_{s_1} - d_{p_1})]^{1/2} \\ &\cdot[\cos^2\alpha\sin^2\beta + \sin^2\alpha\cos^2\beta + \tfrac{1}{2}\sin 2\alpha \\ &\sin 2\beta\cos(d_{s_1} - d_{p_1})]^{1/2}\cdot\cos[(R_{s_2} - R_{p_2}) \\ &+ (d_{s_2} - d_{p_2})]\}^{1/2} \\ &\cdot\sin(\omega t + d_i + d_g + R_{s_3}), \end{aligned} \tag{1}$$

$$\begin{aligned} A_{p3} = A_0\{&\cos^2\alpha(\cos^2\beta\sin^2\gamma + \sin^2\beta\cos^2\gamma) \\ &+ \sin^2\alpha(\sin^2\beta\sin^2\gamma + \cos^2\beta\cos^2\gamma) \\ &+ \tfrac{1}{2}\sin 2\alpha\sin 2\beta\cos 2\gamma\cos(d_{s_1} - d_{p_1}) \\ &+ \sin 2\gamma[\cos^2\alpha\cos^2\beta + \sin^2\alpha\sin^2\beta \\ &- \tfrac{1}{2}\sin 2\alpha\sin 2\beta\cos(d_{s_1} - d_{p_1})]^{1/2} \\ &\cdot[\cos^2\alpha\sin^2\beta + \sin^2\alpha\cos^2\beta \\ &+ \tfrac{1}{2}\sin 2\alpha\sin 2\beta\cos(d_{s_1} - d_{p_1})]^{1/2} \\ &\cdot\cos[(R_{s_2} - R_{p_2}) + (d_{s_2} - d_{p_2})]\}^{1/2} \\ &\cdot\sin(\omega t + d_i + d_g + R_{p_3}). \end{aligned}$$

In these equations, the $A_0$ is the amplitude of the electric vector, the $\omega$ is $2\pi$ times the frequency of the incident light, and the $d_i$ and $d_g$ the phase of the incident light and the increase in phase due to passage through the prism. The $\alpha$, $\beta$, and $\gamma$ are the azimuth angles for each of the three resolutions of the electric vector about the two perpendicular directions, and the $d_{s_1}$, $d_{s_2}$, $d_{p_1}$, $d_{p_2}$ the phase changes after reflection for the perpendicular and parallel components at the first and second roof surfaces. $R_{s_2}$, $R_{p_2}$, $R_{s_3}$, and $R_{p_3}$ are given by

$$\tan R_{s_2} = \frac{\cos\alpha\cos\beta\sin d_{s_1} - \sin\alpha\sin\beta\sin d_{p_1}}{\cos\alpha\cos\beta\cos d_{s_1} - \sin\alpha\sin\beta\cos d_{p_1}}$$

$$\tan R_{p_2} = \frac{\cos\alpha\sin\beta\sin d_{s_1} + \sin\alpha\cos\beta\sin d_{p_1}}{\cos\alpha\sin\beta\cos d_{s_1} + \sin\alpha\cos\beta\cos d_{p_1}} \tag{2}$$

$$\tan R_{s_3} = \frac{C\sin(R_{s_2} + d_{s_2}) - D\sin(R_{p_2} + d_{p_2})}{C\cos(R_{s_2} + d_{s_2}) - D\cos(R_{p_2} + d_{p_2})}$$

$$\tan R_{p_3} = \frac{E \sin (R_{s_2} + d_{s_2}) + F \sin (R_{p_2} + d_{p_2})}{E \cos (R_{s_2} + d_{s_2}) + F \cos (R_{p_2} + d_{p_2})}$$

In these relations $C$, $D$, $E$, and $F$ are given by

$$\begin{aligned} C &= \cos\gamma \{\cos^2\alpha \cos^2\beta + \sin^2\alpha \sin^2\beta \\ &\quad - \tfrac{1}{2}\sin^2\alpha \sin 2\beta \cos(d_{s_1} - d_{p_1})\}^{\frac{1}{2}} \\ D &= \sin\gamma \{\cos^2\alpha \sin^2\beta + \sin^2\alpha \cos^2\beta \\ &\quad + \tfrac{1}{2} \sin 2\alpha \sin 2\beta \cos(d_{s_1} - d_{p_1})\}^{\frac{1}{2}} \end{aligned} \tag{3}$$

$$\begin{aligned} E &= \sin\gamma \{\cos^2\alpha \cos^2\beta + \sin^2\alpha \sin^2\beta \\ &\quad - \tfrac{1}{2} \sin 2\alpha \sin 2\beta \cos(d_{s_1} - d_{p_1})\}^{\frac{1}{2}} \\ F &= \cos\gamma \{\cos^2\alpha \sin^2\beta + \sin^2\alpha \cos^2\beta \\ &\quad + \tfrac{1}{2} \sin 2\alpha \sin 2\beta \cos(d_{s_1} - d_{p_1})\}^{\frac{1}{2}} \end{aligned}$$

If this same plane polarized monochromatic light wave is permitted to enter the lower half of the prism aperture and to emerge from the upper, a similar set of equations can be written with the $\alpha$, $\beta$, and $\gamma$ replaced by $\delta$, $\epsilon$, and $\eta$, the corresponding azimuth angles for each of the vector resolutions along this path. These equations correspond to the waves indicated in Fig. 11 by $a_{s_2}$ and $a_{p_2}$. The equations for $a_{s_3}$ and $a_{p_3}$ as well as the auxiliary equations corresponding to Eqs. 2 and 3 are of exactly the same form so need not be written here.

It perhaps should be emphasized that the preceding equations are applicable only to prisms with uncoated reflecting surfaces for which all the internal reflections occur beyond the critical angle. They will not therefore be useful for silver coated prisms which we will discuss later. It should also be mentioned that if one is considering a three internal reflection roof prism of the form shown in Figs. 1 and 2 (or, for example, a penta-roof prism) the only modification necessary is that of adding a phase factor $d_{s_3}$ to the $A'_{s_3}$ wave and a phase factor $d_{p_3}$ to the $A'_{p_3}$ wave.

To obtain numerical expressions for the four waves emerging from the upper and lower halves of the prism aperture, the only thing missing in Eqs. 1 is a method for determining the phase changes upon reflection. These are determined from Fresnel's Equations which are of the following forms (*1*):

$$\tan \frac{d_s}{2} = \frac{(n_g^2 \sin^2 i - 1)}{n_g \cos i},$$

$$\tan \frac{d_p}{2} = \frac{n_g (n_g^2 \sin^2 i - 1)^{\frac{1}{2}}}{\cos i} \tag{4}$$

The $d_s$ is the phase change in the perpendicular component, and the $d_p$ the phase change in the parallel component. The $i$ is the angle of incidence on the surface in question, and the $n_g$ the refractive index of the glass from which the prism is made. All the quantities in Eqs. 1 can now be determined so that $A_{s_3}$, $A_{p_3}$, $a_{s_2}$, and $a_{p_3}$ can be calculated. For any given initial azimuth angle $\alpha$ (or $\delta$) the ellipticity of the light emerging from the upper and lower halves of the aperture can now be calculated.

## FORMS OF DIFFRACTION PATTERNS FOR PRISMS WITH UNCOATED ROOF SURFACES

To determine the form of the diffraction pattern which such a prism will produce, we are now confronted with a rather unusual problem. Referring now to Fig. 11, we can see that we have four plane waves at the right travelling in a direction upward from the plane of the figure, all of which have different amplitudes and phases (see Eqs. 1). We must now place over these four plane waves a lens and bring all these waves to a common focus, and then calculate the form of the diffraction pattern for different azimuth angles.

Before we could calculate the form of the diffraction pattern characteristic of four such waves, it became necessary to investigate the simpler problem of calculating the diffraction pattern for only two such waves. This is, of course, a problem in Fraunhofer Diffraction and the classical procedures are well established for calculating the forms of these diffraction patterns when the amplitude and phase of a single wave is constant over a single aperture, or over multiple apertures of the same form, often used to represent a diffraction grating. Here, however, we have two adjacent apertures in which the amplitudes and phases of the two waves are different and they also may be polarized with their electric vectors in

planes either parallel or perpendicular to each other. These problems are apparently new.

The problem of predicting the form of the diffraction pattern for plane polarized waves with parallel electric vectors in the upper and lower halves of the aperture having different amplitudes and phases is very similar to a problem solved by Airy (*2*) in 1841. If a white light source is observed with the usual type prism spectrometer, one of course sees a continuous spectrum. If, however, the telescope aperture is limited to a small square aperture, and a piece of mica of uniform thickness is placed over half this aperture, the spectrum is crossed by a series of dark lines referred to as Talbot's Bands (*3*). In explaining the presence of these bands Airy was also faced with calculating the form of the diffraction pattern when the amplitudes and phases of the two unpolarized waves (in the two halves of the aperture) were different. The treatment of the problem which we have presented for single plane polarized waves in the two halves of the aperture is a simplified version of Airy's more complicated problem, for in his solution he calculated the diffraction pattern forms outside the focal plane in the transition region between Fraunhofer and Fresnel Diffraction.

I shall not burden you with the details of the mathematics. To calculate the forms of the diffraction patterns it is necessary first to write down the equations for the two parallel plane polarized waves in the two regions of the aperture with their different amplitudes and phases. These two waves must then be integrated over their respective regions of the aperture in accordance with the usual methods of Fraunhofer Diffraction. After the integrations were carried out and various simplifications made, the following equation was found for the diffraction pattern form.

$$J = \frac{(4ab)^2}{4} \cdot \frac{K^2}{F^2} \cdot \frac{\sin^2 U}{U^2} \cdot \frac{\sin^2 (V/2)}{(V/2)^2} \cdot [A_0^2 + 2\bar{A}_{s_2}\bar{a}_{s_2} \cos (V - \delta)] \tag{5}$$

In this equation, $A_0$ is the initial amplitude of the electric vector of the plane polarized light, $\bar{A}_{s_2}$ and $\bar{a}_{s_2}$ the amplitudes of the electric vectors of the two parallel components in the two halves of the aperture, $\delta$ the difference in phase between the two waves, and $K$ an arbitrary constant. The $U$ and $V$ are the usual diffraction angles defined by

$$U = \frac{2\pi a\xi}{\lambda F}, \qquad V = \frac{2\pi b\eta}{\lambda F}, \tag{6}$$

where the $a$ and $b$ are the half width and half length of the diffracting aperture in Fig. 11, $\xi$ and $\eta$ are the coordinates in the focal plane at the point for which the intensity $J$ is being determined, $\lambda$ is the wave length, and $F$ the effective focal length of the focusing lens. In checking these considerations experimentally, we considered only the case for which $\bar{a}_{s_2} = \bar{A}_{s_2}$. For this special case Eq. 5 reduces to

$$J = (4ab)^2 \cdot \frac{K^2}{F^2} \cdot \bar{A}_{s_2}^2 \cdot \frac{\sin^2 U}{u^2} \cdot \frac{\sin^2 V/2}{(V/2)^2} \cdot \cos^2 \frac{(V - \delta)}{2}. \tag{7}$$

If we consider waves in the upper and lower halves of the aperture with their electric vectors polarized perpendicularly to each other such as $A_{s_2}$ and $a_{p_2}$ in Fig. 11, the diffraction pattern form is calculated as before by integrating over the two regions of the aperture. However, when the electric vectors are perpendicular to each other, the diffraction patterns characteristic of each half of the aperture would not be expected to interact. On this basis then, the resultant diffraction pattern characteristic of the complete aperture would be expected to be a superposition of the diffraction patterns characteristic of each of the two halves. Considerations of this sort led to the following equation for the diffraction pattern for this particular case.

$$J = \frac{(4ab)^2}{4} \cdot \frac{K^2}{F^2} \cdot \frac{\sin^2 U}{U^2} \cdot \frac{\sin^2 V/2}{(V/2)^2} (\bar{A}_{s_2}^2 + \bar{a}_{p_2}^2). \tag{8}$$

Again for experimental verification, we assumed that $\bar{A}_{s_2} = a_{p_2}$ so that

$$J = \frac{(4ab)^2}{4} \cdot \frac{K^2 \bar{A}_{s_2}^2}{F^2} \cdot \frac{\sin^2 U}{U^2} \cdot \frac{\sin^2 V/2}{(V/2)^2}. \tag{9}$$

The previous equations predict some

rather interesting results. We will consider first the implications of Eq. 7 for the case in which the electric vectors in the two halves of the prism aperture are parallel to each other. Eq. 7 states that the diffraction pattern in a direction parallel to the horizontal in Fig. 11 (that is, in the $\xi$ direction) is of the usual Fraunhofer form $\sin^2 U/U^2$ shown in Fig. 12. In the vertical direction (that is, in the $\eta$ direction in Fig. 11) the diffraction pattern is a function of $\delta$ and is, in general, unsymmetric. To show the forms of these diffraction patterns, a few calculated patterns have been included for values of $\delta$ from 0° to 270° (see Figs. 13–18). Starting with $\delta = 0°$, we have the usual Fraunhofer Diffraction Pattern. For increasing values of $\delta$, a satellite appears on the left side of the central diffraction maximum. For further increases in $\delta$, this satellite grows and gradually moves to the right while the parent diffraction maximum moves to the right and decreases in size. At the same time it will be noted that alternate bands in the outer structure gradually disappear. At $\delta = 180°$, both the satellite and parent diffraction maxima are of the same intensity, and the outer bands are now twice as wide and twice as far apart. For values of $\delta$ beyond 180°, the former satellite gradually moves into the position of the central diffraction maximum and every other band gradually reappears in the outer band structure. The process is such that for every 360° change in $\delta$, the patterns repeat themselves. If $\delta$ is made to decrease instead of increase, the changes can be made to take place in a reverse order.

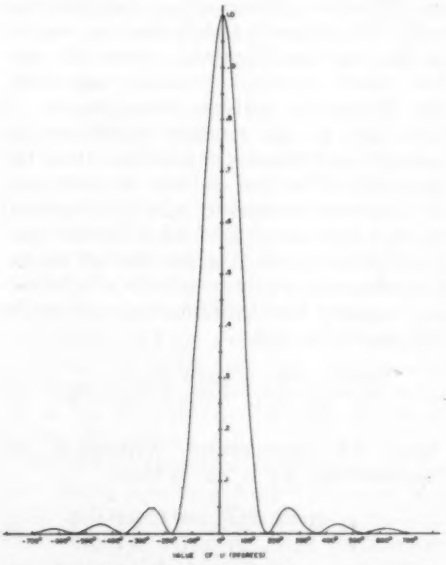

FIG. 12.—Fraunhofer Diffraction Pattern in $U$ direction.

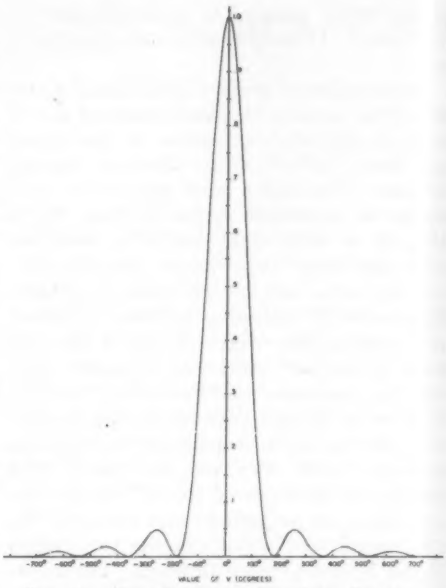

FIG. 13.—Fraunhofer Diffraction Pattern in $V$ direction with $\delta = 0°$.

If the two waves in the two halves of the aperture are polarized with their electric vectors perpendicular to each other as suggested by Eq. 9 the diffraction pattern in the $U$ direction (that is parallel to the horizontal in Fig. 11) is again of the classical Fraunhofer form given by Fig. 12. In the $V$ direction (that is, the vertical direction in Fig. 11), the diffraction pattern is of the form $\dfrac{\sin^2 V/2}{(V/2)^2}$. This diffraction pattern is indicated in Fig. 19. It is of the same form as Fig. 12, but now the central diffraction band is twice as wide and the adjacent maxima are twice as wide and twice as far apart.

To check these theoretical considerations, an experiment (*4*) was performed which

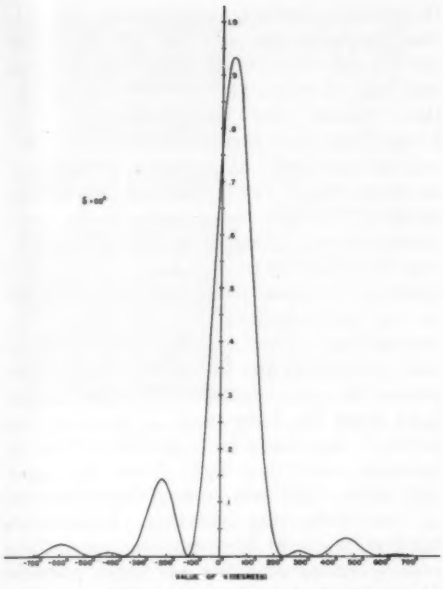

FIG. 14.—Diffraction pattern in $V$ direction for $\delta = 60°$.

we have recommended to several universities having graduate laboratories in physical

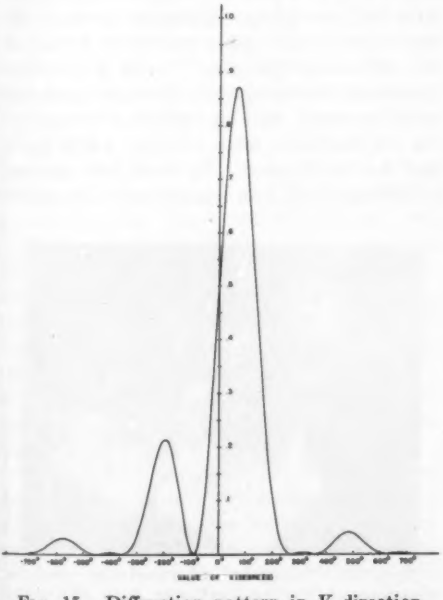

FIG. 15.—Diffraction pattern in $V$ direction for $\delta = 90°$.

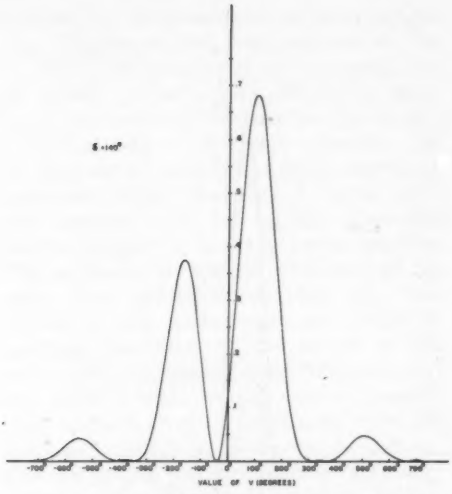

FIG. 16.—Diffraction pattern in $V$ direction for $\delta = 140°$.

optics. This statement is not made because of the author's particular interest, but rather because of what can be learned from this experiment about fundamental diffraction processes. The experiment is of particular interest because of what can be seen. Even after the changes predicted by Figs. 13–18 have been observed for some time, it is rather difficult to determine the overall behavior because so many changes are taking place simultaneously in all parts of the field.

The apparatus used for this experiment is that indicated in Fig. 20. The elements are the same as those used earlier in Fig. 3, but the roof prism is now replaced by a Michelson Interferometer. To fulfill the

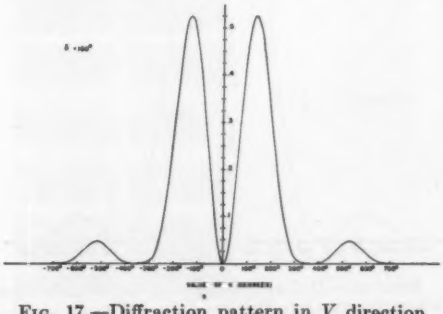

FIG. 17.—Diffraction pattern in $V$ direction for $\delta = 180°$.

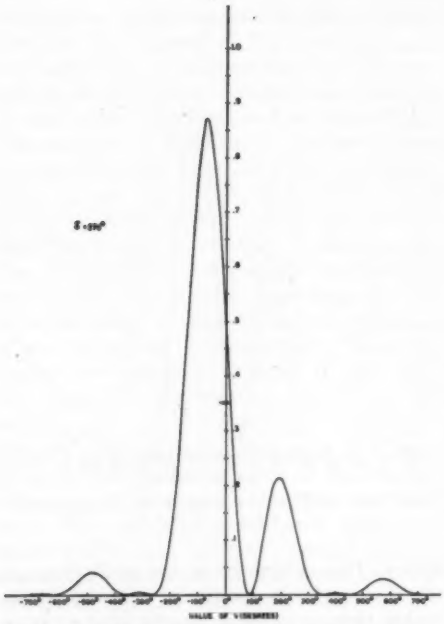

FIG. 18.—Diffraction pattern in $V$ direction for $\delta = 270°$.

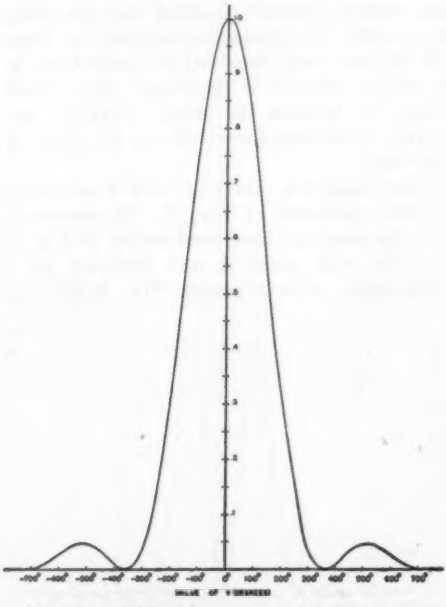

FIG. 19.—Diffraction pattern in $V$ direction when the waves in the two halves of the aperture are polarized perpendicularly to each other.

theoretical conditions suggested by Fig. 11, the interferometer was first adjusted until the central white fringe was in the center of the field of view. One of the mirrors was then rotated until the central Haidinger fringe filled the complete field of view. This adjustment meant that, in the presence of monochromatic light, the amplitude and phase of the light emerging from the interferometer and falling on the square diffracting aperture were constant across this aperture. A razor blade was then inserted in the upper half of the rear arm of the interferometer, and another razor blade was also inserted in the lower half of the right arm of the interferometer. This meant that light from the lower half of the rear arm entered the lower half of the diffracting aperture, and that light from the upper half of the right arm entered the upper half of the diffracting aperture. Interference between the light from the two arms of the interferometer was then no longer possible. However, if now the rear mirror is translated (with no rotation about the horizontal or vertical) the phase of the light in the lower half of the diffracting aperture can be altered at will with respect to that in the upper half, and hence it is possible to introduce arbitrary phase differences between the two waves in the upper and lower halves of the diffracting aperture. If now a polarizer is inserted between the collimator and the interferometer and is oriented properly, the conditions set forth by Fig. 11 and Eq. 7 can be established. To establish similar conditions for Eq. 9, a good half wave plate

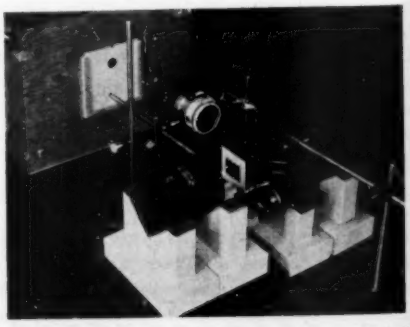

FIG. 20.—Photograph of apparatus used for obtaining diffraction patterns with Michelson Interferometer.

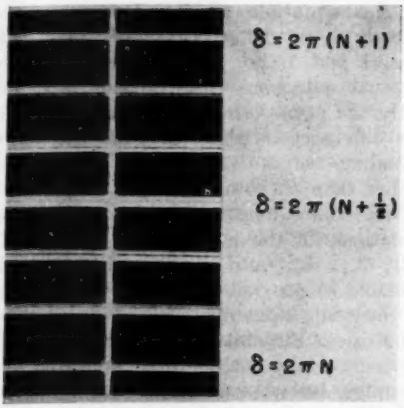


FIG. 21.—Forms of central diffraction bands with Michelson Interferometer.

can be inserted over either the upper or lower half of the emerging aperture.

To show the forms of these diffraction patterns, when the electric vectors in the two halves of the aperture were polarized in parallel directions, photographs were taken in the focal plane of the focusing lens for various differences in phase between the waves in the upper and lower halves of the diffracting aperture. Attempts were made to adjust the exposures so as to show the changes both in the central band structure and in the outer band structure. Fig. 21 shows the forms of the central bands. If we start at the bottom of the figure with a phase difference of some multiple of $2\pi$ between the waves in the upper and lower halves of the aperture, and then gradually move the rear interferometer mirror, the central horizontal band splits into two bands and then goes back together again as predicted by the theory. No changes take place in the vertical central diffraction band. In Fig. 22 every other band in the outer band system disappears and then reappears as the rear interferometer is translated. This again is in agreement with the previous equations.

These pictures, although showing the general behavior of these bands, are no substitute for direct observation. With the eye, many more bands can be seen. The behavior of the complete band system can best be described by relating it to a single row of soldiers. The intensity of the light emitted by these soldiers, or their brightness, is symmetrical with respect to the soldier in the middle of the row and falls off rapidly to both sides. When the interferometer mirror is translated, all the soldiers start marching in the same direction but as they march alternate soldiers gradually disappear. They disappear, however, in a very curious way, for all the remaining soldiers appear to be very much brighter. The soldier in the middle of the row at the same time gradually divides into two soldiers of the same brightness. With increasing movement of the mirror in the same direction, the marching continues, but now soldiers begin to reappear in alternate positions and grow in brightness while the previous soldiers decrease in brightness. The two central bright soldiers are gradually replaced by a single soldier whose brightness is about twice that of the previous two. These changes keep repeating as long as the interferometer mirror is moved in the same direction. If its direction is reversed, the soldiers reverse their direction of march and all the previous changes take place in a reverse order.

Similar experimental justification was sought for Eq. 9 for which the two electric vectors in the upper and lower halves of the aperture were polarized in directions perpendicular to each other. To obtain this a good half wave plate was inserted over half of the square diffracting aperture. When this was done and a photograph

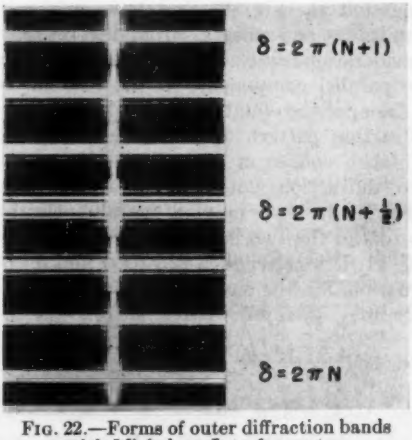


FIG. 22.—Forms of outer diffraction bands with Michelson Interferometer.

taken of the diffraction pattern, the result was that shown in Fig. 23. This diffraction pattern was fixed in form and showed no changes with the movement of the interferometer mirror. The horizontal central diffraction maximum is twice that of the vertical, and the adjacent secondary diffraction maxima in the horizontal direction are twice as wide and twice as far apart as the corresponding secondary maxima in the vertical direction. These experimental facts are in accordance with Eq. 9 and Figs. 12 and 19.

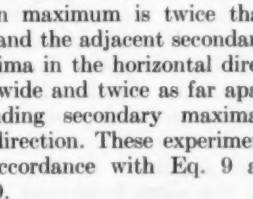

FIG. 23.—Diffraction pattern form when waves in two halves of aperture are polarized perpendicular to each other.

Having learned something about the methods for calculating the forms of the diffraction patterns when the electric vectors in the two halves of the aperture are polarized parallel and perpendicular to each other, we were now able to return to the original roof prism problem and solve the problem of determining the form of the diffraction pattern when there are two waves in each of the two halves of the aperture which are polarized perpendicularly to each other as suggested by Fig. 11 and have arbitrary amplitudes and phases. From the previous considerations it was quite clear that only the parallel components in the two halves of the aperture could interact. The resultant diffraction pattern for the complete prism will then consist of a super-position of the two diffraction patterns characteristic of each of the two pairs of parallel electric vectors in the two halves of the aperture in Fig. 11. If we refer then to Eqs. 1 and 5, the equation for the complete diffraction pattern may then be written as follows:

$$J = (4ab)^2 \cdot \frac{K^2}{F^2} \cdot \frac{\sin^2 U}{U^2} \cdot \frac{\sin^2 V/2}{2(V/2)^2} \cdot \{A_0^2 + \overline{A}_{s_2}\bar{a}_{s_2}\cos[V - (\mathcal{R}_{s_2} - \mathcal{R}_{s_1})] + \overline{A}_{p_2}\bar{a}_{p_2}\cos[V - (R_{p_2} - R_{p_1})]. \quad (10)$$

In this equation, all the quantities have already been defined in connection with Eqs. 1 and 5. For roof prisms with three internal reflections this equation is of exactly the same form, because in Eq. 5 it is the difference in phase between the corresponding waves which is of importance rather than their absolute phases.

With this equation and the corresponding equations for the quantities $A_{s_2}$, $a_{s_2}$, $A_{p_2}$, $R_{s_2}$, $\mathcal{R}_{s_2}$, $\mathcal{R}_{p_2}$, and $\mathcal{R}_{p_2}$ defined earlier, it is possible to provide numerical values for $J$ by inserting numerical values for all these quantities. Simplification of the problem beyond this point at first appeared too complex, for when attempts were made to substitute theoretical values for these quantities (see Eqs. 1, 2, 3) in the above equation the expansions became tedious to handle. In our first paper (*5*) on this subject relating to the three internal reflection roof prism described by Figs. 1 and 2, numerical values for each of these quantities were inserted directly in Eq. 12. The calculated diffraction pattern forms were in qualitative agreement with the experimental forms suggested by Figs. 7 and 8, but no quantitative measurements were made.

During the second phase of the problem, the theoretical considerations were reopened. We tried again to insert theoretical values for each of the quantities in this last equation to obtain an equation for the intensity distribution $J$ which could be expressed directly in terms of experimentally observed quantities. This time we were successful. Again time will not permit my giving the details here. They can be found in the published papers on the subject (*6*). When this was done, however, the following equation for $J$ was found.

$$J = \frac{(4ab)^2 A_0^2 K^2}{F^2} \frac{\sin^2 U}{U^2} \cdot \frac{\sin^2 V/2}{2(V/2)^2} \times \left\{1 + \left[1 - \frac{8n_g^4 \sin^4\tfrac{1}{2}D \cos^2\tfrac{1}{2}D}{[n_g^2(1+\cos^2\tfrac{1}{2}D) - \sin^2\tfrac{1}{2}D]^2}\right]\cos V \quad (11)$$

$$- \frac{4n_g^3 \sin^2\tfrac{1}{2}D \cos\tfrac{1}{2}D[n_g^2(1+\cos^2\tfrac{1}{2}D) - 2]}{[n_g^2(1+\cos^2\tfrac{1}{2}D) - \sin^2\tfrac{1}{2}D]^2(1+\cos^2\tfrac{1}{2}D)}$$

$$[\sin 2\alpha \sin^2\tfrac{1}{2}D - 2\cos 2\alpha \cos\tfrac{1}{2}D]\sin V\}.$$

From Table I, the angle $\theta$ which the $S_1$ vibration makes with the plane of Fig. 9 is given by

$$\cos\theta = \frac{1}{(\cos^2(D/2)+1)^{\frac{1}{2}}} \tag{12}$$

It is now quite easy to fix the azimuth angle $\alpha$ of the entering plane polarized light with respect to this $S_1$ vibration. To calculate the form of the diffraction pattern when plane polarized light is incident on such a generalized two or three internal reflection roof prism with uncoated reflecting roof surfaces, it is necessary now to know only $n_g$, $D$ and $\alpha$. In normal usage the prism is usually illuminated by unpolarized light. The corresponding equation for $J$, when the prism is illuminated by unpolarized light, can be found from this last equation. If the incident light is completely unpolarized, then all values of $\alpha$ are equally probable. Assuming this to be the case, this last equation for $J$ can be integrated and averaged for all values of $\alpha$ between 0° and 180°. This means that an integral of the form

$$\frac{1}{\pi}\int_0^{\pi} J\, d\alpha$$

must be evaluated. When this integration is carried out terms involving sin $2\alpha$ and cos $2\alpha$ will be found to vanish. In unpolarized light the form of the diffraction pattern will then be expected to be given by

$$J = (4ab)^2\frac{A_0^2K^2}{F^2}\cdot\frac{\sin^2 U}{U^2}\cdot\frac{\sin^2(V/2)}{2(V/2)^2}$$
$$\left\{1+\left[1-\frac{8n_g^4\sin^4(D/2)\cos^2(D/2)}{[n_g^2(1+\cos^2(D/2))-\sin^2(D/2)]^2}\right]\cdot\cos V\right\} \tag{13}$$

Eqs. 11 and 13 describe all the properties of the diffraction patterns for two and three internal reflection roof prisms, when all reflecting surfaces are uncoated.

It may be of interest now to see what these equations tell us about the diffraction properties of such prisms. From both of these equations, the first remark which we can make is that the diffraction patterns in a direction parallel to the horizontal in Fig. 11 or in the plane containing the roof edge will, for both polarized and unpolarized light, always be of the classical Fraunhofer form $\frac{\sin^2 U}{U^2}$ for all values of $D$, $n_g$, and $\alpha$. In the vertical direction in Fig. 11 or in a direction perpendicular to the roof edge, the pattern for polarized light is a function of $n_g$, $D$, and $\alpha$ and for unpolarized light it becomes a function of $n_g$ and $D$. Since Eq. 11 is unsymmetrical in $V$ and Eq. 13 symmetrical in $V$, it follows that the diffraction pattern in the $V$ direction for polarized light will, in general, be unsymmetrical and in unpolarized light, symmetrical.

In discussing the particular forms of these diffraction patterns, in the $V$ direction, it is more convenient to discuss first the patterns produced by unpolarized light. If the prism is to have its maximum resolving power characteristic of an aperture of width $2b$ in Fig. 11, then it is clear that the $V$ dependent part of Eq. 13 should reduce to the Fraunhofer form $\frac{\sin^2 V}{V^2}$. The only way this is possible is for the coefficient of the cos $V$ term to reduce to unity. For a fixed value of $n_g$, the only values of $D$ for which the coefficient of the cos $V$ term will reduce to unity are $D = 0°$, and $D = 180°$. Referring then to our generalized roof prism in Fig. 9, it is clear that the only two roof prisms with uncoated roof surfaces, which will produce normal diffraction patterns characteristic of an aperture of width $2b$, are then one which returns the light in the direction from which it comes and one which allows the incident light to go undeviated. In between these two limiting values of $D$ these roof prisms can be shown to have a maximum of doubling at a value of $D$ given by

$$\sin\frac{D}{2} = \left\{\frac{3n_g^2 - n_g(5n_g^2-4)^{\frac{1}{2}}}{n_g^2+1}\right\}^{\frac{1}{2}} \tag{14}$$

The term doubling of the diffraction pattern may be a bit misleading, particularly for values of $D$ near 0° and 180°. To show just how this doubling of the diffraction pattern appears as $D$ is changed, several diffraction patterns were calculated from Eq. 13 using only the $V$ dependent terms. The forms of these diffraction patterns, with ordinates multiplied by two, can be seen in Fig. 24. The values of $D$ being used are indicated to the right of each of the

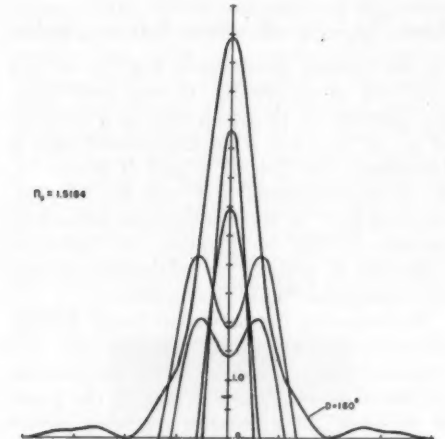


FIG. 24.—Form of diffraction patterns in unpolarized light in the $V$ direction for roof prisms with uncoated roof surfaces having different angular deviations $D$ at roof edge.

patterns, and the refractive index $n_g$ used was 1.5184 corresponding to the value for the green mercury line for the particular glass used. For a value of $D = 0°$, the diffraction pattern is of the usual Fraunhofer form shown earlier in Fig. 13. Up to values of $D = 60°$ in this figure, the changes are not too pronounced for all the secondary bands can still be seen in the outer band structure. At $D = 90°$ every other band in the outer band structure has disappeared, and the central band is now materially broader. For $D = 120°$ and 135° the central diffraction band splits into two separate bands with a distinct minimum at the center. Every other band in the outer band structure is also absent. The $D = 120°$ pattern is the diffraction pattern which this theory predicts for the three internal reflection roof prism in Figs. 1 and 2. If this pattern is considered in conjunction with the Fraunhofer pattern in Fig. 12 it can be seen that Eq. 13 at least predicts the general features of the diffraction pattern for this prism appearing in Fig. 7. For larger values of $D$, the diffraction pattern form in Fig. 24 rapidly goes over again into the Fraunhofer Pattern. At $D = 160°$ the doubling in the central band has already disappeared, and the outer bands are starting to divide into

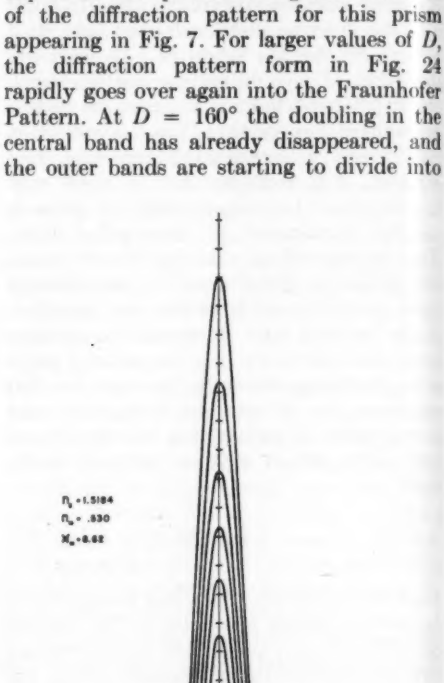


FIG. 25.—Form of diffraction patterns in unpolarized light in the $V$ direction for roof prisms with roof surfaces coated with silver and having different angular deviations $D$ at the roof edge.

the band system characteristic of the Fraunhofer Diffraction Pattern. The term doubling of the diffraction pattern in this paper refers then either to a broadening or splitting of the central band of the form in Fig. 24.

The form of the diffraction pattern in polarized light for prisms of arbitrary $D$ given by Eq. 11 is a little more complicated to discuss. As stated before, in the $U$ direction the pattern is of the classical Fraunhofer form. In the $V$ direction the pattern will, in general, be unsymmetric and will repeat itself for every 180° change in $\alpha$. These changes in the diffraction pattern are such that the oscillations in form take place about the pattern in unpolarized light. For $D = 0°$ and $D = 180°$ the term containing the $\alpha$ disappears so that prisms with these values of $D$ always produce a Fraunhofer Diffraction Pattern in the $V$ direction for both polarized and unpolarized light. In the more general case about all that one can say is that the larger the deviation of the diffraction pattern from the classical Fraunhofer Pattern in unpolarized light, the larger the asymmetry in the patterns in polarized light.

### FORMS OF DIFFRACTION PATTERNS WITH COATED REFLECTING ROOF SURFACES

All of the previous discussion has been concerned with roof prisms in which the two or three internal reflections take place beyond the critical angle. It now becomes quite interesting to ask what will happen to the diffraction pattern form if the boundary conditions are changed at the roof surfaces. To develop exact equations for this more general case of a prism with arbitrary boundary conditions at the reflecting roof surfaces, it is necessary to start again at the beginning of the previous theory. A plane polarized light wave is again assumed to be incident at the first roof surface in the model (see Fig. 10). The electric vector of this incident wave must again be resolved into parallel and perpendicular components at this surface. After reflection, however, classical electromagnetic theory predicts that both the amplitudes and phases are changed while in the preceding theory only the phases were changed. These reflected components are incident on the second roof surface and must be resolved about the parallel and perpendicular directions for the second roof surface and so on until one arrives at a more complex but similar set of equations to Eqs. 1, 2, and 3. These equations then have to be substituted in Eq. 10. As a result of these rather long mathematical considerations we were successful in finding an equation similar to Eq. 11 for the case in which the prism was illuminated by polarized light. This equation is applicable to all two internal roof prisms, but only to three internal reflection roof prisms in which the third reflection occurs beyond the critical angle and the third reflecting surface is uncoated. This equation is much longer than Eq. 11 so we will not write it down here. The case of more practical interest again is that in which the prism is illuminated by unpolarized light. Such an equation was obtained from the previously mentioned equation by integrating and averaging over $\alpha$ as was done in obtaining Eq. 13 for the uncoated prism. This equation had the following form:

$$J = (4ab)^2 \frac{A_0^2 K^2}{F^2} \frac{\sin^2 U}{U^2} \cdot \frac{\sin^2 (V/2)}{2(V/2)^2}$$

$$\times \left\{ 1 + \frac{4 \sin^4 \tfrac{1}{2}D \cos^2 \tfrac{1}{2}D}{(\cos^2 \tfrac{1}{2}D + 1)^4} \left[ \frac{\sin^4 \tfrac{1}{2}D}{8 \cos^2 \tfrac{1}{2}D} (\rho_s^4 + \rho_p^4) \right.\right.$$

$$\left. - 2 \cos \Phi (\rho_s^3 \rho_p + \rho_s \rho_p^3) - \rho_s^2 \rho_p^2 \right. \qquad (15)$$

$$\left.\left. \times \left( 2 \cos^2 \Phi - \frac{4 \cos^2 \tfrac{1}{2}D}{\sin^4 \tfrac{1}{2}D} \right) \right] \cos V \right\}.$$

In this equation $\rho_s$ and $\rho_p$ are the fractions of the perpendicular and parallel components of the electric vector reflected at each roof surface, and $\Phi$ is the difference in phase between the two components after reflection at each roof surface. This equation is quite general so that it applies to cases in which the reflecting roof surfaces are coated with either dielectric or metallic materials.

The problem of most direct interest, for which the previous equation was useful, was that of calculating the form of the diffraction pattern when the roof surfaces were coated with silver. All the quantities in the previous equation are known except $\rho_s$, $\rho_p$, and $\Phi$. The determination of these quantities becomes a boundary value problem in electromagnetic theory. If the silver

film is assumed to be opaque, and both the glass and silver are looked upon as isotropic homogeneous media, then W. Konig (7) has given equations for these quantities assuming that the boundary layer between the glass and silver is infinitely sharp compared with the wave length. These equations are

$$\tan\Phi = -\frac{2n_g B \sin i \tan i}{n_g^2 \sin^2 i \tan^2 i - (A^2 + B^2)},$$

$$\rho_s^2 = \frac{A^2 + B^2 - 2n_g A \cos i + n_g^2 \cos^2 i}{A^2 + B^2 + 2n_g A \cos i + n_g^2 \cos^2 i}, \qquad (16)$$

$$\rho_p^2 = \rho_s^2 \frac{A^2 + B^2 - 2n_g A \sin i \tan i + n_g^2 \sin^2 i \tan^2 i}{A^2 + B^2 + 2n_g A \sin i \tan i + n_g^2 \sin^2 i \tan^2 i},$$

In these equations the quantities $A$ and $B$ are defined by

$$\begin{aligned} A^2 &= \tfrac{1}{2}\{([n_m^2(1 - \chi_m^2) - n_g^2 \sin^2 i]^2 \\ &\quad + 4n_m^4\chi_m^2)^{1/2} \\ &\quad + n_m^2(1 - \chi_m^2) - n_g^2 \sin^2 i\}, \\ B^2 &= \tfrac{1}{2}\{([n_m^2(1 - \chi_m^2) - n_g^2 \sin^2 i]^2 \\ &\quad + 4n_m^4\chi_m^2)^{1/2} \\ &\quad - n_m^2(1 - \chi_m^2) + n_g^2 \sin^2 i\}. \end{aligned} \qquad (17)$$

$n_m$ in these equations is the refractive index of the metallic coating on the roof surface and $\chi_m$ is its absorption index. Assuming that these films obey these boundary conditions, it is now possible for known values of $n_m$, $n_g$, and $\chi_m$ to calculate the forms of these diffraction patterns. Again in the $U$ direction, we see from Eq. 15 that the diffraction pattern is of the classical Fraunhofer form $\frac{\sin^2 U}{U^2}$. In the perpendicular $V$ direction, about all that we can say from the general form of the equation is that the pattern will be symmetric, for it depends in rather a complicated way on $D$, $n_m$, $n_g$, and $\chi_m$. To show the actual forms of these patterns in the $V$ direction we have included some calculated diffraction patterns in Fig. 25. The values of $n_m$, $n_g$, and $\chi_m$ used were the following:

$$n_g = 1.5184, \qquad n_m = .530, \qquad m = 8.62$$

For a value of $D = 0°$, we see that the diffraction pattern is of the Fraunhofer form $\frac{\sin^2 V}{V^2}$. As $D$ is increased, the central maximum recedes slightly and the minima between alternate bands in the outer band structure rise. For values of $D$ beyond 60°, the patterns do not change much in form for values of $D$ on up to 180°. The angular doubling for roof prisms with coated roof surfaces is theoretically quite small for all values of $D$.

If this figure is compared with Fig. 24 for the unsilvered prism, the advantages and disadvantages of silvering from theoretical considerations can be seen. For values of $D$ up to about 60°, the diffraction pattern is sharper when the roof surfaces are uncoated. From 60° on up to about 160°, the diffraction patterns are sharper with silvered roof surfaces. For values of $D$ beyond 160°, the diffraction pattern again becomes sharper with the uncoated surfaces.

## CALCULATED FORMS OF DIFFRACTION PATTERNS FOR 90° DEVIATION AMICI ROOF PRISM

Having derived this rather detailed theory for calculating the forms of these diffraction patterns, we were very much interested in knowing how this theory behaved in particular cases. In our first paper (5) on this subject, we saw that the theory at least gave a qualitative description of the diffraction patterns both in polarized and unpolarized light for the three internal reflection roof prism in Figs. 1 and 2, when the roof surfaces were uncoated. We now undertook the more delicate experimental problem of trying to obtain a quantitative agreement between theory and experiment when the roof surfaces were uncoated and coated with silver. Since the roof prism in Figs. 1 and 2 was rather an odd-shaped one and not generally available we felt it might be more appropriate to carry out these measurements with the more conventional 90° deviation Amici Roof Prism. This prism, shown in Figs. 26 and 27, is simply a special case of the generalized roof prism in Fig. 9 for which $D = 90°$.

Equations for the diffraction pattern forms in both polarized and unpolarized light, when the roof surfaces are uncoated, can be obtained from Eqs. 11 and 13 by

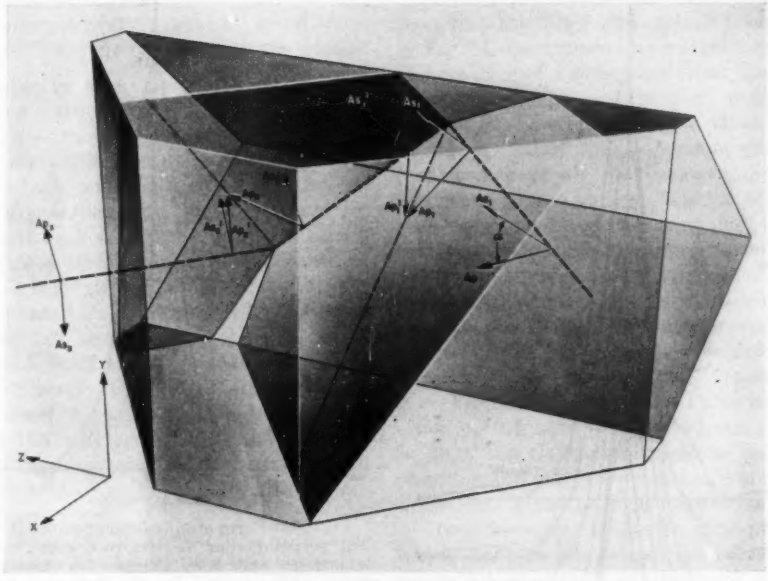

FIG. 26.—Photograph of 90° deviation Amici Roof Prism.

simply inserting $n_g = 1.5184$ and $D = 90°$. Since the diffraction pattern in the $U$ direction has already been established as being of the Fraunhofer form for both polarized and unpolarized light we shall limit our remarks here to a discussion of the pattern in the $V$ direction. When the 90° deviation Amici Roof Prism is illuminated with plane polarized light of various azimuth angles $\alpha$, the patterns resulting from Eq. 11 are those shown in Fig. 28. The changes in the form of the pattern with varying $\alpha$ consist of an oscillation in form back and forth about the zero position of $V$ with a period of 180° in $\alpha$. Similar changes were also found for the earlier three internal reflection prism in Fig. 8 but they were much larger. The corresponding diffraction pattern for unpolarized light obtained from Eq. 13 is shown in Fig. 29. For both polarized light and unpolarized light the expected forms of the diffraction patterns in the perpendicular directions can be obtained by comparing the forms of these last two figures with Fig. 12.

The form of the calculated diffraction pattern for the 90° deviation Amici Roof Prism having roof surfaces coated with silver and illuminated by unpolarized light is arrived at in the same way as those already described in Fig. 25. The same values of $n_g$, $n_m$, and $\chi_m$ were again used. The angle of incidence on the roof surface for this particular prism is 60° and the values of $\rho_s$, $\rho_p$, and $\Phi$ from Eqs. 18 and 19 were

$$\rho_s = 0.9675, \quad \rho_p = 0.8904, \quad \Phi = 226°30'34''$$

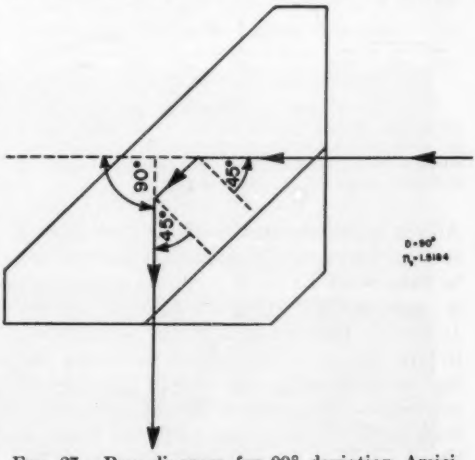


FIG. 27.—Ray diagram for 90° deviation Amici Roof Prism.

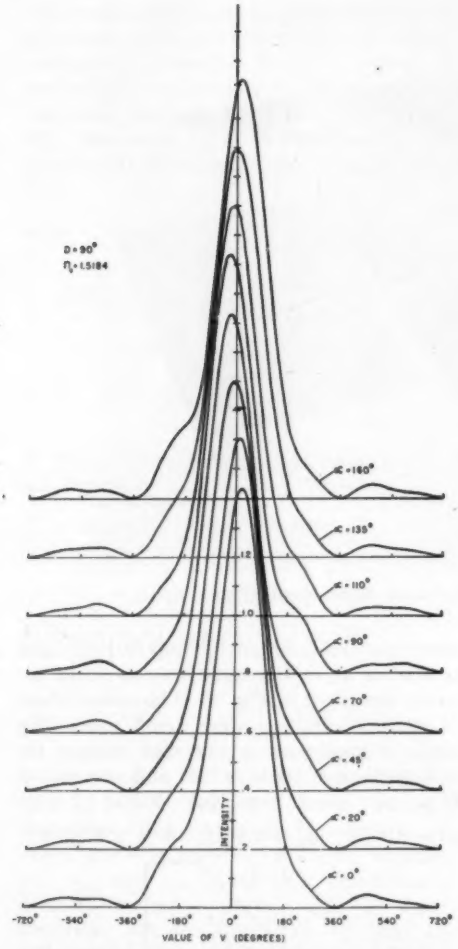


FIG. 28.—Forms of diffraction patterns in a direction perpendicular to the roof edge for a 90° deviation Amici Roof Prism with uncoated roof surfaces when illuminated with polarized light of different entering azimuth angles.

All the quantities in Eq. 15 are then known so that the resultant diffraction pattern can be calculated. In the $U$ direction the pattern is again of the Fraunhofer form in Fig. 12. In the $V$ direction it is of the form shown in Fig. 30. A comparison of these last two figures shows that the theory predicts an increase in sharpness of the diffraction pattern in the $V$ direction when the prism is illuminated by unpolarized light and the roof surfaces are silvered.

FIG. 29.—Form of diffraction pattern in a direction perpendicular to the roof edge for a 90° deviation Amici Roof Prism with uncoated roof surfaces illuminated by unpolarized light.

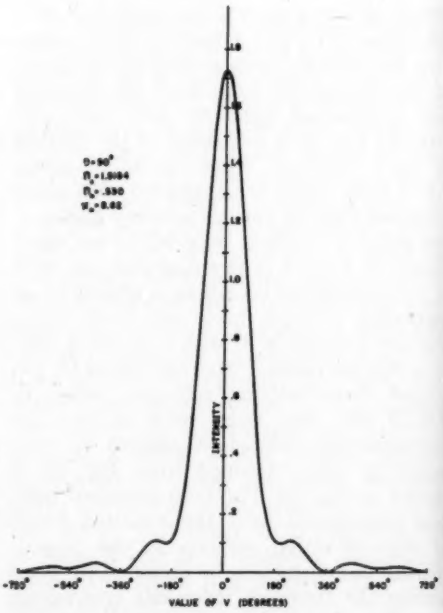


FIG. 30.—Form of diffraction pattern in a direction perpendicular to the roof edge for a 90° deviation Amici Roof Prism having silver coated roof surfaces and illuminated by unpolarized light.

### EXPERIMENTAL METHODS FOR DETERMINING THE DIFFRACTION PATTERN FORM FOR THE 90° DEVIATION AMICI ROOF PRISM

To observe the previously calculated diffraction pattern forms an optical system having the components shown schematically in Fig. 31 was set up in the laboratory. An AH4 high pressure mercury arc source, rotatable polaroid, and suitable filters for isolating the green mercury line were placed in front of a 10-micron slit as indicated at the left in the figure. The light from this slit was collimated by a 492 mm E.F. telescopic objective and then entered the 90° deviation Amici Roof Prism at the right. After passage through this prism the emerging light passed through a five mm square aperture centrally placed behind the prism, and was then brought to a focus by a 3,350 mm E.F. lens so as to magnify the diffraction pattern.

A photograph of the actual apparatus used is shown in Fig. 32. For making quantitative measurements on these diffraction patterns, the filter and polaroid suggested in Fig. 31 was replaced by a Gaertner monochromator and a polarizing Glan Thompson nicol prism. These can be seen mounted at the left in the figure. Early in these experiments we found that vibration was quite troublesome so all the various units were mounted on two optical benches which in turn were mounted on a double I beam structure. This combination proved to be rigid enough so that photographs of the diffraction pattern could be taken. The photographs themselves were recorded with a conventional 35 mm camera with the lens removed. This experimental arrangement gave Fraunhofer Diffraction Patterns of the order of 0.4 mm between adjacent bands so that the diffraction patterns in the $V$ direction for the 90° deviation Amici Roof Prism were about twice as wide (see Fig. 29).

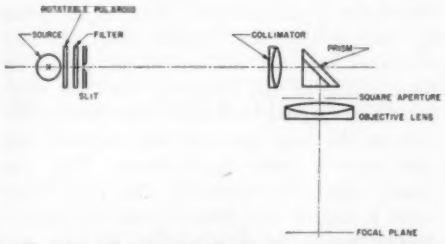


FIG. 31.—Schematic diagram of optical system used for observing diffraction patterns for 90° deviation Amici Roof Prism.

There were several experimental problems which had to be solved before we were successful in obtaining agreement between the calculated and experimentally observed diffraction patterns. I shall mention only a few of these. One of the most troublesome of these was that of finding a proper mount for the prism. The prism not only had to be mounted at the proper height and orientation, but it also had to be free from strain to obtain the proper diffraction pattern. The mount finally adopted is shown in Fig. 33. The prism itself was lightly but firmly clamped to a machinist's V-block by a specially made Lucite C-clamp. The

FIG. 32.—Photograph of complete optical system.

machinist's V-block was mounted on a base plate, which assured us that the height of the prism was always correct, and that its entering face was perpendicular to this base plate. Rotation of this combined unit about a vertical axis made it possible, by autocollimation methods, to line up the entering surface of the prism so that it was normal to the entering light rays. This prism mount gave us a strain free diffraction pattern providing all the prism surfaces were also carefully cleaned. Centering the diffracting aperture with respect to the prism also proved troublesome. It was found quite early that the diffraction pattern form could be changed by simply moving this aperture along the vertical bar seen in Fig. 33. The approximate height of this aperture could always be determined by placing it behind the prism and observing the Fresnel Diffraction Pattern of this aperture with an eyepiece (see Fig. 5) in a plane behind the focusing lens and making vertical adjustments until the dark band was at the center of this pattern. Final adjustments of this height were made with the micrometer until the diffraction pattern in the focal plane of the focusing lens was symmetric in unpolarized light. The determination of the focal plane of the focusing lens also was a little troublesome. This was finally done by replacing the roof prism with a mirror and making careful adjustments until the Fraunhofer Pattern was obtained. These patterns were actually microphotometered to be sure that the proper position was obtained. We also encountered the usual difficulties found when attempts are made to make quantitative measurements with photographic materials. I shall not elaborate on these here, for they can be found in both the published paper (*6*) on this subject as well as in other places. It will be sufficient here to say that on each film with a diffraction pattern photograph, we placed a density calibration. A microphotometer trace of one of these diffraction patterns and the density calibration can be seen in Fig. 34. Both of these tracings were made with a Leeds and Northrup recording microdensitometer. The procedure for relating the experimental and theoretical diffraction patterns is indicated in

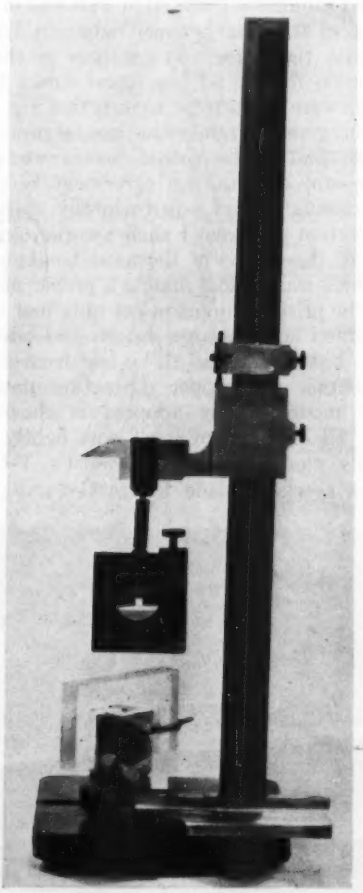

FIG. 33.—Photograph of prism and diffracting aperture mount.

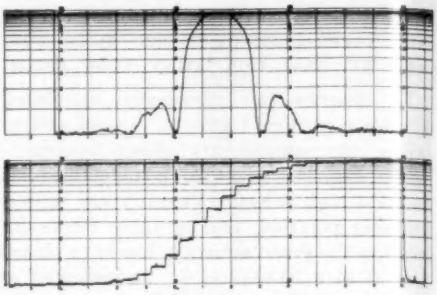

FIG. 34.—A typical microphotometer trace of a diffraction pattern and density calibration.

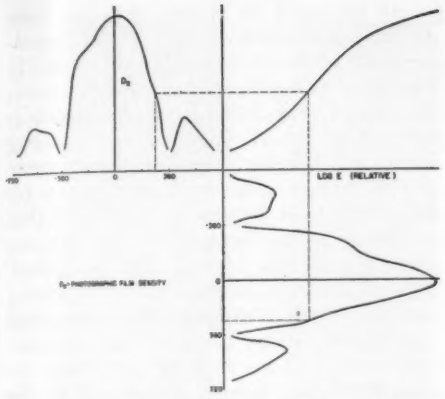

FIG. 35.—Method of converting experimental diffraction pattern to calculated Log $E$ pattern.

Fig. 35. The microphotometered diffraction pattern is indicated schematically at the upper left. To transform this microphotometered pattern to the corresponding theoretically calculated pattern plotted on a log $E$ basis, the ordinates of all the points on this curve must be transformed to the abscissae on the theoretical curve at the lower right, in the manner indicated by the dotted line, using the $D$-Log $E$ curve for the film.

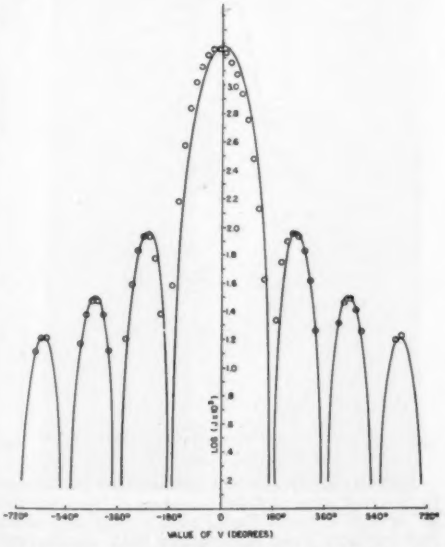

FIG 36.—Experimental and theoretical forms of Fraunhofer Pattern plotted on Log $E$ basis.

Before we could carry out these experiments, we first had to obtain a 90° deviation Amici Roof Prism of high quality. Errors in roof angle could not be tolerated, for these would also produce a doubling of the image.

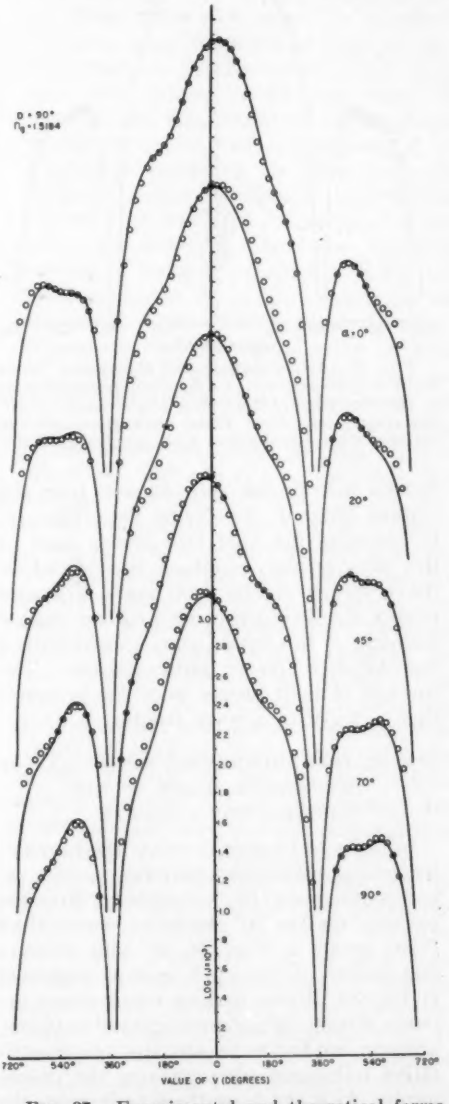

FIG. 37.—Experimental and theoretical forms of diffraction patterns in a direction perpendicular to the roof edge plotted on Log $E$ basis for 90° deviation Amici Roof Prism with uncoated roof surfaces when illuminated with plane polarized light of entering azimuth angles $\alpha$.

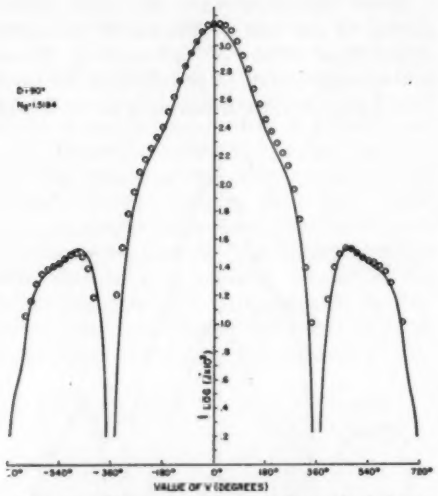


FIG. 38.—Experimental and theoretical forms of diffraction patterns in a direction perpendicular to the roof edge plotted on a Log $E$ basis for 90° deviation Amici Roof Prism with uncoated roof surfaces when illuminated with unpolarized light.

Several such prisms were obtained from the Optical Shop of the Naval Gun Factory. In choosing the final two prisms used in this work primary emphasis was placed on the accuracy of the roof angle. The two prisms finally chosen showed no visible doubling of the image when viewed with a one hundred power autocollimator. The surfaces of both prisms were flat to better than a tenth of a wave length.

## CORRELATION BETWEEN EXPERIMENTAL AND THEORETICAL FORMS OF THE DIFFRACTION PATTERNS

In order to be able to relate the previous theoretical diffraction patterns to the experimental ones, the calculated diffraction patterns for the 90° deviation Amici Roof Prism given in Figs. 28, 29, and 30 were first plotted on the log $E$ basis as suggested in Fig. 35. Before making comparisons between theoretical and experimental patterns, however, we had to be sure that our quantitative techniques were yielding the proper results. As a check on these techniques the Fraunhofer Diffraction Pattern in Fig. 12 was first subjected to these tests. The result of this plot and the experimentally observed points indicated by circles, obtained from the microphotometer trace of the experimentally observed pattern, are shown in Fig. 36. The agreement between the calculated curve and the experimental points is fairly good. If we found a corresponding agreement between the calculated curve and the experimentally observed points for the Amici Roof Prism, we concluded that the theory for the formation of these diffraction patterns was adequate for this prism. Figs. 37 and 38 show the type of agreement obtained in the $V$ direction when the prism was illuminated by polarized and unpolarized light, and its roof surfaces were uncoated. These figures indicate that the theory describes these diffraction patterns within the error obtainable from the experiment. Fig. 39 shows the type of agreement obtained in the $V$ direction when the prism was illuminated with unpolarized light and its roof surfaces coated with silver. Clearly the agreement is not as good in this case, for the observed pattern is sharper than the corresponding calculated one. Although we cannot definitely say why this disagreement exists, we do have some general ideas on

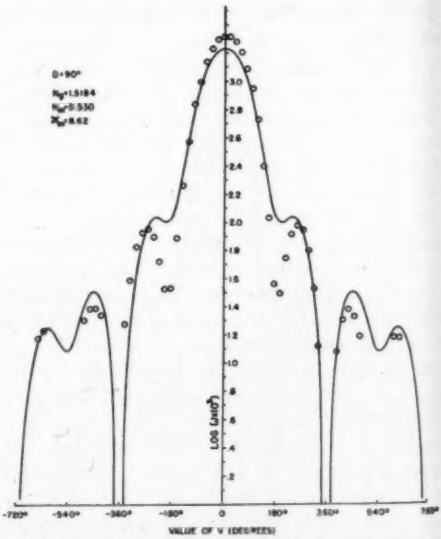


FIG. 39.—Patterns in a direction perpendicular to the roof edge plotted on a Log $E$ basis for the 90° deviation Amici Roof Prism with silver coated roof surfaces when illuminated with unpolarized light.

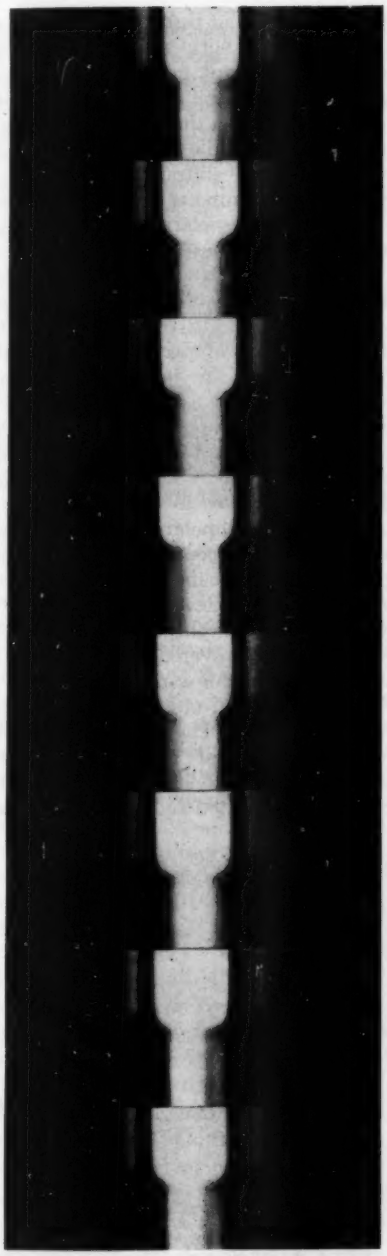

FIG. 40.—Photograph of diffraction patterns in a direction perpendicular to roof edge for 90° deviation Amici Roof Prism with uncoated roof surfaces when illuminated with polarized light of different entering azimuth angles $\alpha$.

the subject. The films used on these prisms were all of the chemically deposited type which were covered with a plastic type preservative and black paint to prevent deterioration. The optical constants used for these films were those for chemically deposited films as measured from the glass silver surface. By the author's own admission these values are not very exact. We therefore feel that we did not have sufficient knowledge of just what is happening at the glass-silver boundary for these particular films to calculate the form of the diffraction pattern with sufficient exactness. It is possible, for example, that the boundary conditions assumed in arriving at the previous equations for $\rho_s$, $\rho_p$, and $\Phi$ are not applicable here. The optical constants themselves may be considerably in error for these particular films and they may also be partially transparent. These things will not be known until actual experimental measurements are made on each of these quantities. There is also a possibility that an error exists in the theory, for the only check we have on its correctness is that of setting $\rho_s = \rho_p = 1$ and forcing it over into the equations for the unsilvered prism. We have also tried the optical constants normally given for evaporated films of silver, but the discrepancy is a little larger in this case. At present then, all we can say is that the theory for the diffraction pattern form for roof prisms with silvered surfaces gives results for these particular films which are in the direction of the observed experimental patterns, but the discrepancy between the calculated and observed patterns is outside of our experimental error.

In the next two figures we have tried to sum up for you photographically the results of these observations on the 90° deviation Amici Roof Prism. In Fig. 40 there is a series of photographs of diffraction patterns mounted side by side so as to show the changes in shape of these patterns in the $V$ direction, when the prism is illuminated with polarized light of different azimuth angles, and the roof surfaces are uncoated. Two patterns can be seen simultaneously. In taking these photographs half the length of the 10 micron slit was covered with a filter which decreased the light from one-

half of the slit so that the changes in the forms of the central band, as well as the outer band system, could be seen at the same time. The changes which take place in this photograph are in agreement with the changes predicted in Figs. 28 and 37. At the left in Fig. 41 are shown the diffraction patterns in the two perpendicular directions when the roof surfaces are uncoated and the prism is illuminated by unpolarized light. Clearly the horizontal pattern is much broader than the corresponding vertical one, and the outer bands in the horizontal pattern are twice as wide and twice as far apart as the corresponding bands in the vertical pattern. If now the roof surfaces are silvered, the vertical diffraction pattern in this figure remains the same, but the horizontal pattern changes into the pattern seen in the third picture from the left. At the extreme right in this picture the Fraunhofer Diffraction Pattern is given. It will be noted that this pattern is essentially of the same shape as the second and third photographs. These patterns are so nearly of the same shape that it requires a microdensitometer to show up the differences.

## CONCLUSIONS

As a result of this paper we are led to the quite important conclusion that all perfectly made two and three internally reflecting roof prisms with uncoated reflecting roof surfaces, except prisms with $D = 0°$ and $D = 180°$, exhibit a doubling of the diffraction pattern in a direction perpendicular to the roof edge, while in a plane containing the roof edge the diffraction pattern is of the classical Fraunhofer Form. If the incident light is plane polarized this doubling is unsymmetric and its form is influenced by the entering azimuth angle of the plane polarized light. The forms of these diffraction patterns for both two and three internally reflecting roof prisms with uncoated roof surfaces can now be calculated from a knowledge of the *angular deviation at the roof edge*, the *prism refractive index*, and the *incident azimuth angle of the plane polarized light*, if the prism is illuminated by plane polarized light. When the prisms are illuminated with unpolarized light silvering the roof surfaces decreases this doubling in a direction perpendicular to the roof edge except for prisms near $D = 0°$ and $D = 180°$. The forms of the diffraction patterns for prisms with silvered roof surfaces can also be calculated for unpolarized light if the *refractive index* and *absorption index* of the silver are known. The agreement between the calculated and observed diffraction patterns for the 90° deviation Amici Roof Prism with uncoated roof surfaces is about




FIG. 41.—Photographs of diffraction patterns in unpolarized light when roof surfaces are uncoated and coated with silver.

as good as could be hoped for, but when the roof surfaces are coated with silver the agreement is not satisfactory. However, even with these questionable values for the optical constants of the silver and perhaps the questionable boundary conditions at the glass-silver surface the theory still predicts the general forms of the changes found.

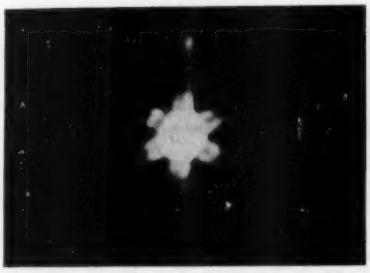

FIG. 42.—Photograph of diffraction pattern for three corner prism.

I should also say a few words about the remaining unsolved problems relating to this subject. The final equations in this paper were limited to the diffraction patterns only in the focal plane of the focusing lens, and no attempt has been made to calculate the forms of the observed patterns out of this plane. These equations also apply only to rays which are incident on the roof surfaces at the same angle of incidence. We therefore do not know anything about the forms of the diffraction patterns when the rays travel through the prism in oblique directions such that the rays fall on the two roof surfaces at different angles of incidence. Patterns off the axis of the focusing lens but with their central horizontal band confined to the plane of Fig. 31 can still be calculated from the theory presented here by making corrections for refraction at the entering and emergent surfaces and considering the angle $D$ to have a different value. All the previous patterns have been calculated assuming that the limiting aperture was always a square. In actual usage this may not always be the case so that the forms of these patterns may be modified somewhat. It would be particularly interesting to repeat these calculations when the lens is the limiting aperture so that circular and semicircular apertures become necessary. This theory has only been applied to roof prisms of two different geometries. Obviously, these studies ought to be extended to other uncoated prisms of different $D$'s before we can conclude that the theory is correct for all values of $D$. The previously mentioned problem of what happens at the roof surfaces when they are silvered needs further study to determine whether or not the theory is correct for the prisms with coated roof surfaces. The theory itself needs to be extended to include three internal reflection roof prisms having all three surfaces coated with silver. Mr. D. C. Harper (*9*) of the Eastman Kodak Company has recently made some experimental observations which show that single roof surfaces, when coated with aluminum, tend also to minimize the doubling of the type discussed here. This problem has not been considered. Throughout the paper it has always been assumed that the prism under consideration always has a perfect 90° roof angle. This raises the subject of what happens to the image when there is also a small amount of doubling present due to a small error in the roof angle. There are therefore many phases of this problem which still remain unsolved.

Before leaving this subject of unsolved problems in this field, I would like to show you the form of the diffraction pattern characteristic of the three-corner prism used to send light back in the direction from which it comes. This prism is familiar to all of you and has many uses. This problem is very closely related to the previous problem, but is in general even more complicated. If we consider a circular limiting aperture, some preliminary considerations show that one must consider six equal apertures forming 60° sections of the circle, each of which contains two waves polarized with their electric vectors perpendicular to each other having different amplitudes and phases. This diffraction pattern (see Fig. 42) was photographed by Donald Lowe of this Laboratory using a monochromatic point source. The explanation of this particular diffraction pattern still remains to be worked out.

ACKNOWLEDGMENTS

The author acknowledges the assistance of several people who made contributions in one way or another to the preparation of this paper. First of all he is indebted to the late Max Zwillinger of the Optical Shop at the Naval Gun Factory for originally suggesting this problem. Several of the preliminary investigations on this problem were carried out in conjunction with Mr. Zwillinger. The Optical Shop of the Naval Gun Factory was responsible for the making of the unusually fine prisms used in this work. The care exercised in their making can only be appreciated when attempts are made to duplicate them. Various groups with the Naval Ordnance Laboratory also made substantial contributions. The Analysis and Publications Divisions were responsible for routine calculations, curve plotting, and the art work associated with this paper. The Photographic Division made all the photographic reproductions. Various other members in the Division helped from time to time on various phases of the work. The author also is indebted to H. Osterberg of the American Optical Co. and F. Zernicke of the University of Gronigen in Holland who checked various parts of the theory by independent methods.

REFERENCES

(1) BORN, M. *Optik*: 43. Berlin, 1933.
(2) AIRY, G. B., Phil. Trans. Roy. Soc. London **130** (pt. 2): 225. 1840; **131** (pt. 1). 1841.
(3) TALBOT, F. H. London Edinburgh Phil. Mg. **10**: 364. 1837.
(4) MAHAN, A. I.: Journ. Opt. Soc. Amer. **37**: 852. 1947.
(5) MAHAN, A. I., Journ. Opt. Soc. Amer. **35**: 623. 1945.
(6) MAHAN, A. I. AND PRICE, E. E. Journ. Opt. Soc. Amer. **40**: 664. 1950.
(7) KONIG, W. *Handbuch der Physik*, **20**: 202–207, 240–243. Berlin, 1928.
(8) TATE, J. T., Phys. Rev. **34**: 327, 1912.
(9) HARPER, D. C. Paper 20, Thirty-Eighth Annual Meeting, Optical Society of America, Rochester, N. Y., Oct. 15–17, 1953.

## ENTOMOLOGY.—*New Saldidae (Hemiptera) from the Old World.* CARL J. DRAKE, Iowa State College, Ames, Iowa.

The present paper contains the descriptions of five new shore bugs or Saldidae from Africa and India. I am indebted to Dr. W. E. China, of the British Museum (Natural History), London, for the privilege of studying many saldids from various regions of the world. The types of the new species are deposited in the British Museum. In the descriptions, the ocular micrometer scale and magnification are such that 80 units of length or width equal one millimeter. I am also indebted to Mr. Arthur Smith, artist of the above Museum, for the fine drawing of the type of *Saldula championi*, n. sp.

**Chiloxanthus sangchana**, n. sp.

Large, black, slightly shining, without color markings; pubescence moderately dense, very short, reclining, not very conspicuous. Head black, considerably flattened in front, with only a small pale spot near the inner excavation of each eye; ocelli pale, not elevated, with the space between them about equal to the diameter of an ocellus; width across eyes, 1.25 mm. Antennae black, shortly pilose, with only a small subapical spot on second segment brownish testaceous, measurements—I, 21; II, 130; III, 81; IV, 80. Legs black, the middle and hind femora with a long, narrow, testaceous or brownish stripe on the front face of each; pubescence and spine-like hairs black; tarsi with some testaceous on dorsal surface of segments II and III.

Pronotum broad, slowly narrowed anteriorly, with lateral margins rectate, with some bristly hairs on anterior third of outer margin, deeply roundly excavated behind, three times as wide at base as median length (180:60), with front margin much narrower than basal width (100:180); callus large, little elevated, with a shallow discal impression; about three times as long as hind lobe, marked off behind by a shallow transverse furrow; collar very narrow. Scutellum slightly convex, scarcely wider at base than median length (128:120), nearly smooth, indistinctly rugulose, with a deep transverse impression at the middle. Hemelytra wide, with surface faintly rugulose; membrane lightly clouded with fuscous, with veins darker, composed of four cells, the fourth cell shorter than bordering cell, not reaching the peripheral vein.

Length, 6.25 mm; width, 1.50 mm.

*Type* (female), Sangcha, north of Kamaon, India, elevation 14,500 feet, H. G. Champion.

This species does not fit into the "Synopsis Specierum Subgenera *Chiloxanthus* Reuter" as keyed by Kiritshenko, Ann. Mus. Zool. Acad. Sci. **16:** 545–546, 1916. It appears to be closest to *C. lama* Kiritshenko and *C. kozlovi* Kiritshenko, both from Tibet.

**Calacanthia tibetana,** n. sp.

Head black, with calloses next to eyes and frontal callosities flavous; ocelli small, yellowish, slightly elevated, separated by less than half of the diameter of an ocellus; eyes large, grayish brown, with a few very short hairs. Antennae rather stout, blackish fuscous with the inner sides of I and II flattened and testaceous, densely pilose with some scattered longer hairs; segments I and II stouter than others, with the pubescent hairs bordering pale flattened side whitish, with only a few stiff brown bristles on flavous surface, measurements—I, 30; II, 56; III, 36; IV, 40. Rostrum long, extending between hind coxae, brownish testaceous. Body beneath blackish with acetabula whitish testaceous and the posterior margins of ventrites whitish. Legs flavotestaceous; femora with posterior side and conspicuous spots (arranged in rows) dark fuscous; tibiae armed with long, dark brownish fuscous, stiff, bristly spines, which are placed on small dark fuscous spots, tips of tibiae also infuscate; tarsi with the short basal segment and also apical half of third dark fuscous.

Pronotum black, slightly shining, finely rugulose, moderately narrowed anteriorly, with exterior margins nearly straight and narrowly margined (above and beneath) with flavous, more than twice as wide at base as median length (110:40); pubescence moderately dense, decumbent, grayish; callus large, not very high, not extending laterally on explanate margins, with a large, deep, discal impression; hind lobe short, scarcely half as long as callus, deeply broadly excavated behind. Sculellum large, very little convex, finely rugulose behind, transversely impressed at the middle, black slightly shining, with pubescence somewhat golden apically. Hemelytra rather dull, dark fuscous with a bluish tinge, clothed with short, somewhat fallen, golden pubescence; clavus without pale marks; corium quite variable in amount of flavous, with a few small flavous spots or with most of outer corium and outer part of inner corium partly flavous; membrane dusky flavous, with four cells, each cell with fuscous spots.

Length, 4.25–5.00 mm; width, 2.00–2.25 mm.

*Type* (macropterous male) and *allotype* (macropterous female), Supi River, Tibet, under stones, altitude, 15,000 feet, H. G. Champion. Paratypes: 7 specimens, same data as type.

Separated from *C. trybomi* (J. Sahlberg) by the flavous legs with fuscous markings, less elevated callus, shorter second antennal segment and lack of sparsely scattered long hairs on dorsal surface of hemelytra.

**Saldula championi,** n. sp. (Fig. 1)

Elongate, black, slightly shining, with prominent testaceous markings as described in structures; dorsal surface clothed with fine, erect, pale hairs, the hairs more numerous on hemelytra. Head black, with a pale testaceous spot near the rounded excavation of each eye, with the usual long hairs; frontal callosities mostly flavous. Antennae blackish with the first segment and one side of second whitish or testaceous, the

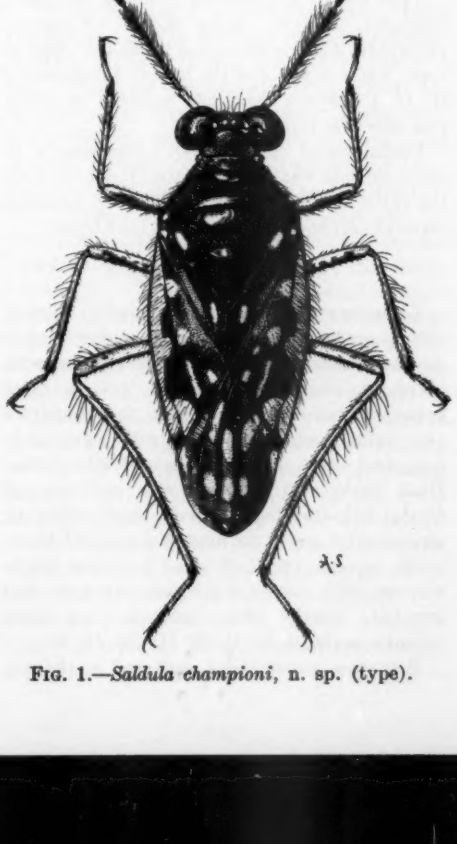

FIG. 1.—*Saldula championi*, n. sp. (type).

fourth segment with a broad band near middle (narrow basal and wider apical part blackish), measurements—I, 32; II, 75; III, 47; IV 43. Ocelli feebly elevated, slightly separated. Width across eyes, 1.05 mm.

Pronotum strongly narrowed anteriorly, deeply excavated behind, with lateral margins straight, with a few erect brownish hairs, the pubescence grayish with a slight golden tinge, recumbent; width at base more than twice the median length (110:40); callus rather high, with a deep discal impression, subequal in length to hind lobe. Hemelytra dark fuscous with pale testaceous marking located as may be seen in the illustration (Fig. 1), rather dull, with some blush areas, color markings a little variable in size; erect hairs brownish with a slight golden lustre, fairly numerous; embolium testaceous with only apex dark fuscous; membrane with four cells, dark fuscous, with pale cellular spots a little variable in size. Legs testaceous with some brownish or fuscous shaded places, quite hairy, especially tibiae and also with longer hairs, the hind tibiae distinctly bowed (Fig. 1); tarsi dark fuscous with second segment testaceous.

Length, 3.90–4.30 mm; width, 1.55 mm.

*Type* (male) and *allotype* (female), Kumaon, Halduani, District, India H. G. Champion. *Paratypes:* 2 specimens, same labels and data as type. Name in honor of the famous Coleopterous H. G. Champion, who has collected so many rare insects in India.

Distinguished readily from other species of genus *Saldula* Van Duzee in the Orient (or even the entire world) by very hairy second antennal segment and bowed, longly hairy hind tibiae.

**Saldula africana,** n. sp.

Elongate-ovate, fuscous-black, slightly shining, with prominent flavous markings as described in structural characters, the hemelytra tinged with bluish; pubescence rather short, grayish, more golden on hemelytra; scutellum and hemelytra also rather densely clothed with moderately long, fine, erect, pale hairs, tinged with golden. Head black, with two spots near each eye and frontal callosities flavous; ocelli small, yellowish, separated by nearly the diameter of one of them; width across eyes, 1.12 mm. Antennae black-fuscous, with only a small pale stripe on first segment, shortly pilose, without long hairs, measurements—I, 30; II, 76; III, 52; IV, 53.

Pronotum moderately narrowed anteriorly, with lateral margins straight, deeply excavated behind, with basal width three times median length (130:45); callus large, rather high, with small discal impression, demarcated both in front and behind by a narrow sulcus (small pits at bottom); collar quite narrow; hind lobe finely rugulose, about one-third as long as callus; explanata margins moderately wide, with a short, submarginal, flavous stripe at middle. Scutellum a little raised, slightly wider at base than median length, transversely impressed near the middle, without color marks. Hemelytra rather dull, with nonbluish area dark velvety fuscous, with embolium almost entirely flavous; clavus with a subbasal and subapical spots flavous; corium with a subbasal, another a little beyond the middle and three or four apical marks flavous; outer corium with an apical spot pale flavous; membrane fuscous with veins darker and a median longitudinal streak in each of the four cells somewhat flavous. Body beneath black, densely clothed with short whitish hairs. Legs long, slender, with pale pubescence; trochanters and margins of acetabula pale testaceous; coxae testaceous; fore and middle femora blackish fuscous with bases and tips somewhat testaceous, the tibiae fuscous with subapical band testaceous, the tarsi black-fuscous; hind femora and tibiae brownish testaceous with some fuscous areas, the tarsi black-fuscous.

Length, 4.75 mm; width, 2.00 mm.

*Type* (male), Nanwamda Valley, Kyanjok, Ruwenzori Range, Uganda, Africa, elevation 6,500 feet; *allotype* (female), Swan River, Mount Elgon, Kenya, elevation 5,000 feet, F. W. Edwards. *Paratypes:* 1 male, same data as allotype, 1 male with type and 1 male, Kilembe, Ruwenzori Range, Uganda, Dec., 1934, F. W. Edwards.

This species may be separated from its African congeners by the elongate form and the somewhat golden hairy clothing of scutellum and hemelytra.

**Saldula capicola,** n. sp.

Moderately large, obovate, black, slightly shining, with hemelytra blackish fuscous and prominently marked with flavous or brownish flavous spots (two spots on clavus, four spots on inner corium, and apical spot on outer corium), almost entire embolium and also a narrow marginal stripe on each side of pronotum flavous. Legs blackish fuscous with trochanters, base of femora, most of dorsal face of tibiae and

second tarsal segments testaceous or brownish testaceous. Pubescence short, grayish, somewhat golden on hemelytra. Venter black, slightly shining, with hind margin of segments narrowly testaceous. Female unknown.

Head black with the two calloses near each eye and frontal callosities flavous; width across eyes, 1.15 mm. Antennae black-fuscous, shortly pilose, measurements—I, 30; II, 55; III, 46; IV, 46. Pronotum moderately obliquely narrowed anteriorly, with outer edge rectate, broadly roundly excavated behind, with basal width three times median length (130:40); callus moderately large, not extending laterally on explanata margins, set-off by the usual transverse sulci, with discal impression slightly in front of middle, about one and a half times as long as hind lobe. Scutellum a little convex, with the usual transverse impression near the middle, slightly wider at base than median length (90:80). Hemelytra with flavous embolium edged along the margin with fuscous; membrane with four cells, dark fuscous, with two or three whitish spots in each cell.

Length, 4.00 mm; width, 0.90 mm.

*Type* (male), Witte Esbosch, on rockface trickling with water, South Africa, Jan. 10, 1927, G. E. Hutchson. *Paratypes:* 2 males, same data as type.

This species is smaller than *S. africana*, n. sp., and lacks the hairy clothing on dorsal surface of body.

## ENTOMOLOGY.—Ayurakitia, *a new genus of mosquito from northern Thailand* (Diptera: Culicidae). DEED C. THURMAN, JR.[1] (Communicated by Ernestine B. Thurman.)

This new genus is proposed for a single Northern Thailand species, the males of which in general appearance seem similar to the males of the genus *Aedes* but differ morphologically in lacking postspiracular bristles. The presence of a fringe on the squama and the absence of both spiracular and postspiracular bristles bring the species into close relationship with those of *Haemagogus*, *Heizmannia*, *Ficalbia*, and *Mansonia* (*Coquillettidia*). However, *Haemagogus* and *Heizmannia* have the anterior pronotal lobes enlarged and all *Heizmannia* and some species of *Haemagogus* bear tufts of hair on the postnotum; *Ficalbia* have the proboscis swollen at the apex; and *Mansonia* (*Coquillettidia*) have distinct tibial bristles, and are large yellowish mosquitoes, while the new species has normal pronotal lobes, a bare postnotum, a normal proboscis, and no tibial bristles, and the specimens are small with silvery markings. Superficially the males somewhat resemble the males of *Paraedes*, although the distinct generic characters of *Paraedes* (squama bare, postspiracular bristles present, and no lower mesepimeral bristles) serve to distinguish the two.

While this species is being separated from the genus *Aedes* on the lack of postspiracular bristles, Aitken (1941) erected *Kompia*, a lower Sonoran region subgenus of *Aedes*, for specimens (females) without postspiracular bristles, reporting that *Kompia* was closely related to the subgenus *Finlaya*, differing only in the absence of this character. Vargas (1950) relegated *Kompia* to synonymy under the subgenus *Ochlerotatus* based only on the structures of the male terminalia, disregarding the accepted subgeneric characters for females of *Ochlerotatus* (cerci long, eighth abdominal segment narrow and completely retractile) though females of *Kompia* are obviously different.

Should the absence of postspiracular bristles be disregarded and the new species be placed into the genus *Aedes* (following Aitken, 1941), the structures of the male terminalia would show a close affinity to *Aedes* (*Finlaya*) in lacking a basal lobe on the basistyle, and to *Aedes* (*Aedimorphus*) in that the dististyle is highly modified; but differing from *Finlaya* in having a simple claspette without an articulated appendage, and from *Aedimorphus* by possessing a

[1] Sanitarian, Division of International Health, United States Public Health Service, assigned as Regional Malaria Control Adviser for Northern Thailand with the U. S. A. Operations Mission to Thailand (USOM) of the Foreign Operations Administration. (This paper was submitted for publication by Mrs. Ernestine B. Thurman after the death of the author. Mr. Thurman died suddenly in Chiengmai of illness contracted while on duty in Northern Thailand only nine days prior to the completion of his assignment.)

claspette. However, the females of the new species can not be placed into any one of the subgenera of *Aedes* as listed by Edwards (1932), differing from *Finlaya* by having the eighth abdominal sternite not large and prominent; from *Ochlerotatus* by having the cerci short and the eighth abdominal segment broad and not completely retractile; from *Aedes* by being a light colored species with ornamentation and with upright scales on the head; from *Aedimorphus* by having a banded proboscis; and from *Christophersiomyia* by having broad, semi-erect scales on the anterior pronotal lobes. From *Kompia* the new species differs by having one lower mesepimeral bristle, setae on the head, and the postspiracular area without scales.

With the combination of characters as observed, it is impossible to place the Northern Thailand species into any of the presently recognized subgenera of *Aedes* or genera of Culicidae. Therefore, it seems more appropriate to erect a new genus, without attempting to expand the concept of the known genera, until additional information is obtained about the relationship of this species to others.

**Ayurakitia,** n. gen.

Genotype: *Ayurakitia griffithi*, n. sp.

Diagnostic characters: Margin of squama with fringe. Anterior pronotal lobes normal, well separated. Spiracular and postspiracular bristles absent. Pulvillus absent.

Subordinate characters: Male palpus slightly shorter than proboscis; female palpus one-sixth as long as proboscis. Wing membrane with distinct microtrichia at 45 ×; vein 6 extending well beyond the base of the fork of vein 5; wing scales: Squame scales blunt, plume scales rounded at tip. Anterior pronotal lobe with long brown bristles, and without scales. Posterior pronotal lobe with several strong bristles and without scales. Postspiracular area without scales. One lower mesepimeral bristle well developed.

Male terminalia: Basistyle three times as long as wide with neither a subapical nor a basal lobe. Dististyle highly modified, less than one-half as long as basistyle. Tenth sternite narrow, curved, bladelike, ending in a sharp point. Claspette long, slender, spiralled, with one short and two long setae at apex.

**Ayurakitia griffithi, n. sp.**

*Male:* Small species of light golden coloring with yellow and pale golden scales and dark brown hairs. Pleura and sides of abdomen with silvery spots. Tarsi with basal silvery bands. Head: Dorsal surface mostly covered with flat golden scales, a row of silvery scales adjacent to eyes, a row of curved, dark brown bristles curving forward on anterior portion; centrally and posteriorly a patch of dark brown, upright scales. Proboscis dark brown with a ring of golden scales centrally, golden scales scattered from base to golden ring, dark apically. Clypeus bare, pale straw-colored. Palpus slightly shorter than proboscis, with few hairs, dark on basal and two apical segments; segments between these with light golden scales mixed with light brown scales. Antenna almost as long as palpus, normal, with long pale hairs; apical segments elongated and darker; basal segments pale.

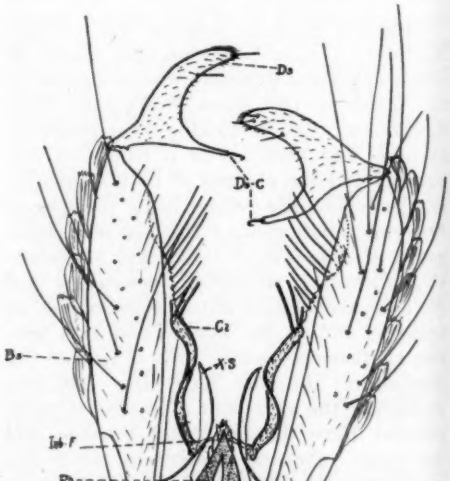


FIG. 1.—Structures of male terminalia of *Ayurakitia griffithi*, n. sp.

B-P, Basal Plate
Bs, Basistyle
Cl, Claspette
Ds, Dististyle
Ds-C, Claw of Dististyle
Inb-F, Interbasal Fold
IX-T, Ninth Tergite
Ix T-L, Lobe of Ninth Tergite
Ph, Phallosome
Pm, Paramere
X-S, Tenth Sternite

Thorax: Mesonotal integument light brown with thin, curved, appressed, dark brown scales and dark brown, short, curved setae. Tubercles for dorsocentral and prescutellar bristles present but most of these bristles missing. Integument of anterior pronotal lobe without scales, pale and clear with six long, dark brown bristles and two large posterior-pronotal bristles. Pleural integument without dark areas, light brown on upper portion and light golden toward coxae; patches of large, broad, silvery-white semi-erect scales on the following sclerites; propleuron, upper and lower portions of sternopleuron, upper mesepimeron, and meron. Wing 3 mm. Anterior and posterior fork cells of wings fairly long. Anterior fork longer than stem. Veins with moderately thick scaling, fairly broad, brown scales especially on anterior veins, scaling thinner toward tips; plume scales thin, elongate, rounded; squame scales blunt. Legs: Foreleg, femur dark brown scaled above, pale golden posteriorly and ventrally with a tiny tip of few silvery scales; tibia with dark brown scales above, pale golden posteriorly and ventrally; first tarsal segment equal to length of remaining segments, an anterior basal patch of silvery white scales not quite encircling the segment, a similar patch at the base of the second segment, remaining segments dark; large claw with a thin blunt tooth; small claw simple. Midleg, anterior surface dark brown scaled, a spot of silvery scales just beyond the middle of the femur; femur silvery tipped, ventrally pale golden; tibia dark anteriorly, pale golden ventrally and posteriorly except at apex; first and second tarsal segments silvery scaled basally, remainder of tarsal segments dark scaled; large and small claw simple. Hindleg, femur dark anteriorly with a silvery spot just beyond the middle, posteriorly and ventrally pale scaled except for the dark tip; tibia with an indefinite, broad ring of silvery scales, dark-ringed apically; all tarsal segments with a basal ring of silvery scales, except segment 5 which is all dark; claws small and simple. Halteres pale with capitellum dark scaled. Abdomen: Integument light golden scaled, with an indefinite triangle of brown scales centrally and apically on each segment, brown scales extending onto lateral margins, encircling a patch of silvery iridescent scales on each segment.

Terminalia: Basistyle three times as long as wide, outer surface covered with long, ridged scales rounded apically, long setae, and fine spicules; ventral edge with an area of dense setae beyond the middle. Dististyle less than half the length of basistyle; narrow at base with two indentations on inner surface; expanded from base to a wide apex; apex with a deep, central concavity; ventral arm curving toward concavity, clothed in fine setae; surface of concavity with setae and spicules to dorsal arm; dorsal arm narrow, bearing a retrose, spinelike claw; distance between arms at apex is equal to length of dististyle. Claspette not reaching middle of basistyle, narrow, half-spiralled with apex toward basistyle; apex rounded bearing two long setae, and a few minute setae; spiculations to base and on inner basal fold. Tenth sternite narrow, curved, bladelike. Phallosome simple, open at base; dorsal surface with lateral triangular flanges anterior to middle, ventral surface narrow with six fingerlike points from apex to base. Paramere triangular in shape; rounded basally; pointed apically; laterally expanded beyond middle. Basal arm broad and rounded, tapering sharply, curving abruptly into a long point. Ninth tergite with definite apical lobes each bearing two setae; concave medially; basal surface with deep concavity medially forming a bridge between the lobes.

*Female:* Coloration and size similar to male. Head: Palpus dark scaled, about one-sixth the length of proboscis. Proboscis dark scaled apically; pale ring not complete, upper surface dark brown scaled. Antenna normal, almost as long as proboscis; 4 or 5 dark hairs in whorl at base of each segment, and many short hairs on each segment; integument dark. Torus dark brown. First flagellar segment with few small, dark setae. Occiput similar to male. Thorax: Mesonotal integument similar to male. Scutellum rubbed, only a few dark brown scales remaining on lobes. Wing veins more heavily scaled than the male, scales dark brown with slight copperish luster. Pleura rubbed, silvery scales remaining on propleuron, upper and lower portions of sternopleuron, and upper mesepimeron. Legs: Foreleg, golden scaled with a few scattered dark scales; some long brown setae; femur golden scaled; first and second tarsal segments dark with white basal bands; other segments dark. Last three tarsal segments missing from hind leg, otherwise midlegs and hindlegs same as male. Claws simple.

Holotype male, allotype, seven paratypes,

and two slides of male terminalia: U.S.N.M. no. 62022.

*Type locality:* Doi (mountain) Chom Cheng, a peak of the Doi Sutep Range, Chiengmai Province, Thailand. January 4, 1953, two males (Deed C. Thurman, Jr.); February 14, 1953, one male (Deed C. Thurman, Jr.) and one male and two females (Manop Rattanopradith); February 24, 1953, two males and one female (Deed C. and Ernestine B. Thurman). Specimens were netted while resting on trees in a shaded jungle valley. Immature stages are unknown.

The genus is named in honor of Dr. Luang Ayurakit Kosol, director of the Division of Malaria and Filariasis Control of the Department of Public Health of the Ministry of Health of Thailand, and the species in honor of Dr. Melvin E. Griffith, chief adviser of the Malaria and Filariasis Control Section of the U. S. A. Operations Mission to Thailand, FOA.

The first two males were collected with a net while they were resting on the side of a tree growing in a damp, cool, shady mountain valley at about 3,000 feet elevation, and the other specimens from the same valley during later trips. The valley drops about 100 to 200 feet below the crest of a hill, the site of a rest cabin owned by an American missionary nurse. The hill is known in the local hill-tribe language as "Wong Kut" (meaning an open or cleared peak).

"Wong Kut" is a part of Doi Chom Cheng and Doi Pui, mountain peaks to the northeast of Doi Sutep. The entire range, which is just west of the city of Chiengmai, Chiengmai Province, is known as the Doi Sutep Range after the administrative region of Sutep and collectively the peaks are usually spoken of as Doi Sutep. In order to reach the rest cabin, the collectors climbed a narrow, steep jungle trail from the bottom of the east side of Doi Sutep to midway on the east slope of Doi Chom Cheng. All supplies and equipment were transported by man-carriers. By using the rest cabin as the center of operations, it was possible to do general insect collecting, with emphasis on mosquitoes, for the full length of the trail and on to the summit of Doi Chom Cheng (elevation, 6,000 feet). The jungle was quite dense and the climb too difficult to attempt decending the west side of the mountain; therefore, collections were confined to the more accessible slopes and the valleys on the east side.

The author wishes to express appreciation to Dr. Alan Stone of the U. S. Department of Agriculture, for comparing the specimens; to Mr. Manop Rattanopradith of the Malaria Control Unit no. 4, Chiengmai, for field and laboratory assistance; to Miss Sadie Lemmon of the McCormick Hospital, Chiengmai, for interest and assistance in the project and for the use of her rest cabin; and to Mrs. Ernestine B. Thurman, Malaria Control Training Adviser of the U. S. A. Operations Mission to Thailand, for assistance in all phases of the study.

In addition, I should like to express appreciation to Dr. Luis Vargas of the Institute de Salubridad y Enfermedades Tropicales, México, for lending comparative specimens; to Mr. William H. W. Komp of the National Institutes of Health, for reviewing the manuscript; and to Dr. Melvin E. Griffith, USOM/Thailand, and Dr. Alan Stone for making the completion of this paper possible.—ERNESTINE B. THURMAN.

## REFERENCES

AITKEN, T. H. G. *A new American subgenus and species of* Aedes. Pan-Pac. Ent. **17**(2): 81–84. 1941.

EDWARDS, F. W. *Diptera, family Culicidae.* Genera Insectorum, fasc. 194: 258 pp. 1932.

VARGAS, LUIS. *Los subgeneros de* Aedes. Downsiomyia *n. subgen. (Diptera, Culicidae).* Rev. Inst. Sal. y Enf. Trop. **11**(1): 61–69. 1950.

* * * *

## NOTICE

**An index to the first 40 volumes of the JOURNAL of the Washington Academy of Sciences and the 13 volumes of the PROCEEDINGS has recently been published. Place your order now with Dr. Harald A. Rehder, U. S. National Museum, Washington 25, D. C. Price, $7.50. To members of the Academy, $6.00**